Stockwell Transform Based Medical Image Compression

By

Tewodros Endale

A Master thesis

Presented in partial fulfillment of the requirements for the Degree of Master of Science in Biomedical Engineering

Addis Ababa Institute of Technology
Addis Ababa University

Advisor: Dawit Assefa Haile (PhD)

Co-advisor: Mengistu Kifle (PhD)

Addis Ababa, Ethiopia, November 2017

Declaration

I, the undersigned, declare that this thesis is my original work. It has never been presented for a degree in any other institution and that all sources of materials used in it have been duly acknowledged.

Name: Tewodros Endale Tefera

Signature: ____________________

Date: ________________________

This MSc thesis has been submitted for examination with my approval as an advisor.

____

Dawit Assefa Haile (PhD)

Addis Ababa University

School of Graduate Studies

Certificate of Examination

This is to certify that the thesis prepared by Tewodros Endale Tefera entitled *'Stockwell Transform Based Medical Image Compression'* submitted in partial fulfillment of the requirements for the degree of Master of Science in Biomedical Engineering (Bioinstrumentation and Imaging) complies with the regulations of the University and meets the accepted standards with respect to originality and quality.

Signed by the examining committee

Examiner ____________________________ Signature _______________ Date ______________

Examiner ____________________________ Signature _______________ Date ______________

Advisor _____________________________ Signature _______________ Date ______________

____

Chief of Department or Graduate Program Coordinator

Abstract

S-Transform Based Medical Image Compression

Tewodros Endale

Addis Ababa University, 2017

Image compression is achieved by reducing the redundant and irrelevant data so that the number of bits to represent each image pixel array is reduced. This could be achieved by using transform coding. Images can be transformed from one domain to a different type of representation using some well-known transform. Different types of linear transforms exist in this regard. The Fourier transform and cosine transform are few examples. Multiresolution analysis is becoming important in image analysis and signal processing as it gives resolution on both frequency and time domains, which is not the case in the Fourier and cosine transforms. Wavelet Transform (WT) is the earlies multiresolution member and was proposed on various image processing fields, JPEG2000 image compression tool uses WT. But due to the lack of the absolutely referenced frequency and phase information and sensitivity to noise the application area of WT is limited. The Stockwell transform (S-Transform) is another proposed multiresolution transform that offers the absolutely-referenced frequency and phase information. There exists a very direct relationship between the S-transform and the natural Fourier transform and the S-transform is always invertible. Such advantages of the S-transform inspired many researchers to navigate very useful applications of the transform in different disciplines. But S-transform redundantly doubles the dimension of the original data set making computation expensive and hence the Discrete Orthonormal Stockwell Transform (DOST) was proposed. DOST is a pared-down version of the fully redundant S-transform which reduces the computational cost without changing its multiresolution nature and the absolutely-referenced frequency and phase information.

The proposed image compression scheme in this thesis uses JPEG 2000 image compression scheme as a bench mark. As S-transform outperforms the WT in some useful aspects, WT that is used in the JPEG2000 scheme is replaced by the DOST and a new algorithm has been developed. Compression Ratio (CR), Mean Square Error (MSE), Peak Signal to Noise Ratio (PSNR) and Structural Similarity Index (SSIM) were used to quantify the performance of the proposed compression scheme. Results showed that the DOST allows effective and efficient image compression and outperforms other transform-based approaches including those that makes use of the discrete cosine as well as wavelet transforms. The proposed algorithm has been tested on images acquired from freely available research database and offered an average PSNR, CR, MSE and SSIM of 47.0099, 50.6031, 8.0097 and 0.9295 respectively. In comparison, WT offered an average PSNR, CR, MSE and SSIM of 42.9151, 49.8519, 8.2633 and 0.9108 respectively.

Acknowledgement

St. marry, it is your Love and Intercession with God that gives me life.

I would like to express my gratitude to Dr. Dawit Assefa Haile, my supervisor for his recommendations and support with this paper. Your valuable guidance, constant encouragement and kind help at different stages made me finish this thesis. I am also grateful to my Co-supervisors Dr. Mengistu kifle and Dr. Metasebiya Solomon for sharing their experience and time.

Our PG coordinator, Dr. Masreshaw Demelash, I don't have a word for your comments and your help in all matters. Just thank you. All the staffs of the Center of Biomedical Engineering at Addis Ababa Institute of Technology and my professors, I would like to say thank you for sharing me your experience and for your time. Also, to my classmates, it was fun having you.

I am grateful to all my friends who have given me support and moral for finalizing my thesis. My special thanks goes to my wife Winti, thank you for all you have done. Finally, I would love to say thank you my families, Etesh, Endesh and my sisters, for making me who I am. Without your prayers and support nothing would have been possible.

List of Figures

List of Tables

Acronym

1-D	1-Dimensional
2-D	1-Dimensional
BCH	Bose, Chaudhuri, and Hocquenghem
CALIC	A Context Based Adaptive Lossless Image Codec
CR	Compression Ratio
CR	Computed Radiography
CT	Computed Radiography
DCT	Discrete Cosine Transforms
DCT	Discrete Cosine Transforms
DFT	Discrete Fourier Transforms
DOST	Discrete Orthonormal S Transform
DST	Discrete S – Transform
DWT	Discrete Wavelet Transform
DWT	Discrete Wavelet Transforms
EBCOT	Embedded Block Coding with Optimal Truncation Points
FFT	Fast Fourier Transform
FT	Fourier Transform
JPEG	Joint Photographic Experts Group
JPEG-LS	Lossless Joint Photographic Experts Group
LZW	Lempel-Ziv-Welch
MRI	Magnetic Resonance Imaging
MSE	Mean Square Error
NCD	Non-Communicable Diseases
PACS	Picture Archiving and Communication System
PNG	Portable Network Graphics
PSNR	Peak Signal-To-Noise Ratio
RAC	Relative Address Coding
RLE,	Run Length Encoding
SPIHT	Set Partitioning In Hierarchical Trees
SSIM	Structural Similarity Index
ST	Stockwell Transform
STFT	Short-Time Fourier Transform

TB	Tuberculosis
US	Ultrasound
WHO	World Health Organization
WT	Wavelet Transform

Table of Contents

Chapter One

Introduction

1.1 Background

Medical images are widely used in creating visual representation of internal and external body structures (anatomy) and functional (physiological) parts for use in clinical analysis. The images provide a means of patient information that is dependent on the clinical management of the patient and treatment planning [1]. Based on the images, physicians diagnose the disease type, grade, progression, and/or monitor other important patient treatment outcomes. In the early days, most imaging modalities used conventional films for storage and image retrieval [3]. With the advent of new technologies, nowadays people are moving towards the digital world which decreases the use of films in the application of medical images. The images are acquired at the cost of such as radiation exposure requiring substantial infrastructure, human resource, and patient labor (this especially in the developing world) and the images should be stored, viewed by professionals and shared through a system. Picture Archiving and Communication System (PACS) is one means of storing and uses a server for image transmission through a network. In this regard, compression plays a big role on transmission and storage of digital medical images. Other than PACS, compression has many other vital applications in tele-medicine, tele-radiology applications, real time tele-consultation and the like.

The storage and transmission of medical image data is different from storage and transmission of common visual data for multimedia applications [2]. This is because the compression type used for storing and transmitting of the medical images may lose some relevant information. Losing of data may lead to erroneous diagnostics because of lost data in the compression procedure. Therefore, the type of medical image compression used is very important for efficient archiving and transmission of images.

Compression is defined as the process of coding that will effectively reduce the total number of bits needed to represent certain information [3]. It could be lossy or lossless compression. Lossy compression is a compression technique which losses some information, i.e. the original image is not fully recovered while decompressing. On the other hand, lossless compression has no loss of information i.e. the original image is fully recovered while decompressing. The goal of lossless image compression is to represent an image signed with the smallest possible number of bits without loss of any information, thereby speeding up transmission and minimizing storage requirement [3].

There exist large number of data compression algorithms which have been developed in the literature and, to date many researches are being carried out to come up with better techniques that offer higher compression ratio and better performance. These algorithms can be lossy or lossless and have been developed for different applications. Some of the algorithms are developed for general use. They can be used to compress data of different types (e.g., text files, image files, video files, etc.) [5]. While some of the algorithms are developed to compress efficiently a particular type of files [5]. Some of internationally accepted lossless image compression techniques are summarized as follows:

- Lossless JPEG: it is based on the discrete cosine transform (DCT) predictive image compression algorithm with Huffman or arithmetic entropy coder [3].
- JPEG-LS: low complexity image compression algorithm with entropy coding and the algorithm used is Loco-I [3].
- PNG: predictive image compression algorithm using lz77 and Huffman coding.
- JPEG-2000: based on the wavelet transform image decomposition and arithmetic coding.
- CALIC: based on arithmetic entropy codes

The different compression techniques will be reviewed in the next chapter. The intent of this thesis work was to show the application of an S transform-based image compression scheme for use in efficient and effective storage and transmission of medical images. The scheme involves scalar quantization with thresholding and a lossless entropy encoder of arithmetic coding.

1.2 Statement of the Problem

As countries like Ethiopia are struggling to achieve their development goals, the health sector should be the major contributor to their economic growth. According to the human resource development and administration directorate of the Ethiopian Federal Ministry of Health, the country is one of those in the world with low health workforce density of 0.7 per 1000 population. According to the World Health Organization (WHO), the minimum standard threshold density of health workers is 2.3 per 1000 population. This figure shows Ethiopia is far below the minimum requirement to achieve coverage of primary healthcare.

Not just the obvious communicable tropical diseases including malaria and TB, even non-communicable diseases (NCD) are also becoming increasingly major public health problems as epidemiological transition is progressing in Ethiopia [4]. The number of physicians is significantly small that simply hinders much visible progress in the health coverage across the nation, especially for NCDs, which need specialized physicians. Even the small number of physicians are mainly concentrated in urban areas making health provision services in low resource areas more challenging. Tele-medicine, tele-radiology and tele-consultation are some of the means to alleviate this problem. Storing and transmission of medical images is the basis for such applications and effective and efficient image compression plays a vital role in this regard. For example, the main problem to implement telemedicine is the bandwidth of the transmission system. Due to the increased size and volume of medical images it is difficult to transmit medical images through narrow band width. The other problem with transmission of medical images is security. Patient data is confidential. During image decoding, confidentiality of the patient information should be maintained. After transmission of the encoded (compressed) signal, the decoding (decompression) should be unique. The encoded signal must not be decoded by other decoding technique. Therefore the encoding and decoding (compression and decompression) during image transmission should be efficient and secure. At the same time the medical images ought to be stored and shared over a system. All of these call for the development of a good image compression tool.

1.3 Objectives

1.3.1 General Objective

- To develop a compression algorithm that offers a good compression ratio with high image quality.

1.3.2 Specific Objectives

- To show the application of the S transform in the development of an efficient image compression scheme.
- Develop a lossless compression scheme which can be used in tele-medicine and related applications.
- To test the efficacy of the proposed compression tool in storage and transmission of medical images.
- Compare the efficacy of the proposed compression tool with similar other schemes already proposed in the literature.

1.4 Literature Review

There are many data compression algorithms which have been developed in the literature and, to date many researches are being carried out to come up with newer, better techniques. These algorithms can be lossy or lossless and have been developed for different applications. Some of the algorithms are developed for general use. They can be used to compress data of different types (e.g., text files, image files, video files, etc.) [5]. While some of the algorithms are developed to compress efficiently a particular type of files [5]. In this thesis, we are concerned only with lossless image compression types.

Readers could find details on the basic image compression tools in various literatures. Alarabeyyat et al. in their study proposed a method which combines the LZW (Lempel-Ziv-Welch) algorithm and the BCH (Bose, Chaudhuri, and Hocquenghem) algorithm as an error correcting technique [5]. They have chosen LZW algorithm to reduce the repeated value in images and BCH codes to detect or correct the errors. Their scheme has been tested on a dataset of 20 test images. The result of their algorithm had an average compression ratio of 1.636383. The authors claimed that their proposed algorithm has a better performance compared to the average compression ratios of other algorithms like the RLE, Huffman, and LZW. But their algorithm performed inferior compared to algorithms developed based on the 2-D Discrete Wavelet Transform (DWT) and the fuzzy C-means clustering which offered compression ratios of 2.857 and 1.53 for two different image sets [5, 6]. The lossless compression algorithm proposed by Karras et al. that makes use of the 2-D DWT and the fuzzy C-means clustering achieved high compression rates [6]. However, their algorithm has a problem of blocking effects in the partition boundaries after decompression.

Sungdae Cho et al. applied lossless compression of volumetric medical images with the asymmetric tree 3-D Set Partitioning in Hierarchical Trees (SPIHT) algorithm [7]. SPIHT is a wavelet-based scheme and is considered one of the state-of-the-art algorithms for image compression in the literature. The authors have tested both the symmetric tree 3-D SPIHT and the asymmetric tree 3-D SPIHT algorithms on 8-bit CT and MRI volumetric medical images [7]. Their results showed that the asymmetric scheme performs better than the symmetric tree 3-D SPIHT in terms of bit rates [7]. But they have not compared their scheme against other algorithms with higher compression ratio.

Ramesh and Shanmugam proposed another lossless compression technique based on a wavelet scheme using prediction methods [8]. Two MRI and two CT gray scale standard test image data sets were used for their experiments [8]. They have got higher compression rate than both SPHIT and JPEG2000.

Ukrit et al. conducted an extensive survey on different lossless compression algorithms [3]. They tested JPEG, JPEG-LS, JPEG2000, PNG and CALIC compression techniques on the same image data set. Following their experiments, they concluded that JPEG-LS algorithm has the best performance with best compression ratio and compression speed than the others but JPEG-2000 had higher quality final image [3].

In the present thesis work the wavelet-based methods are the ones bench marked inspired by their best acceptance in the literature. An integral transform with better properties than the wavelet transform is used to develop the proposed image compression algorithm. Its efficacy is checked on selected medical images to show its level of accuracy as well as robustness.

1.5 Organization of the Thesis

The rest of the thesis has been organized in to five chapters. Chapter 2 provides the general introduction on image compression. It discusses the lossy and lossless type of compression with the explanation of the general block diagram. It also discusses different transform based schemes used in image compression. Chapter 3 discusses the basic concepts of the Stockwell (S) transform. It offers explanation about multiresolution analysis. It covers both continuous and discreet S-transforms. Chapter 3 also answers why we use the DOST instead of the fully redundant discreet S- transform. Chapter 4 discusses the proposed compression scheme in this thesis and the methodology involved. Chapter 5 presents the results obtained with important discussions including both the qualitative and quantitative techniques employed to evaluate the performance of the proposed scheme. Finally, Chapter 6 presents concluding remarks and possible feature directions of the study.

Chapter Two

Digital Image Compression

2.1 Introduction

Now-a-days almost all images acquired from different modalities like photographs, MRI, CT scans or any computer-generated images are in digital format. Digital images are designated by two-dimensional pixel arrays and each pixel is represented by the number of bits. But due to the need of large number of bits to represent them, digital images are often bulky. Therefore, digital images need higher storage space, bandwidth, and transmission time and transmission rate. Digital image compression plays a great role in compressing the images so that the storage space, bandwidth, transmission time and transmission rates are lower. Since more and more medical images produced in the hospitals are in digital format, more economical and effective data compression technologies are required [13].

There are various types of redundancies and irrelevant information which exist in pixel values of a digital image. Such are eliminated to reduce the total number of bits required to represents the image [12]. By reducing the redundant and irrelevant data to reduce the number of bits to represent each pixel arrays, the size of the image could be minimized considerably. Hence, image compression could be achieved. Therefore, image compression can be defined as an application of data compression that encodes the original image with fewer bits [15].

Image compression techniques could be either lossless or lossy depending on the requirement we chose. Compared to lossless approaches, lossy techniques offer higher compression ratio. Lossy type of compression technique is most popular compression technique [17]. Lossy compression technique has high compression ratio and allows some acceptable degradation. Therefore, the original image could not be fully recovered during decompression [19]. On the other hand, lossless compression comes with lower compression ratio results but it allows the image to be fully recovered during decompression [19]. For high value images such as medical images where loss of critical information is not acceptable, lossless or visually lossless compression is preferred [15] [19].

Generally, compression can be achieved by removing one or more of the three basic data redundancies [5]:

i. Coding redundancy, which is presented when less than optimal code words are used;
ii. Inter-pixel redundancy, which results from correlations between the pixels of an image;
iii. Psychovisual redundancy (irrelevant information), which is due to data that are ignored by the human visual system [5]. Therefore, eliminating some less relative important information in our visual processing may be acceptable.

Or image compression can be achieved by:

i. Coding methods: which are applied directly to the raw image treating them as a sequence of discrete numbers.
ii. Spatial domain: this method is a combination of spatial domain algorithm and coding methods.
iii. Transform domain: in this model the image is represented using an appropriate basis set. Wavelet transform and DCT (discreet cosine transform) are examples of transform domain methods.
iv. Combination of these methods.

2.2 Lossy Image Compression

Most lossy compressors are three-step algorithms but all three steps are not necessarily included in every compression system [17] [20]. Figure 2.1 shows a general block diagram of lossy compression.

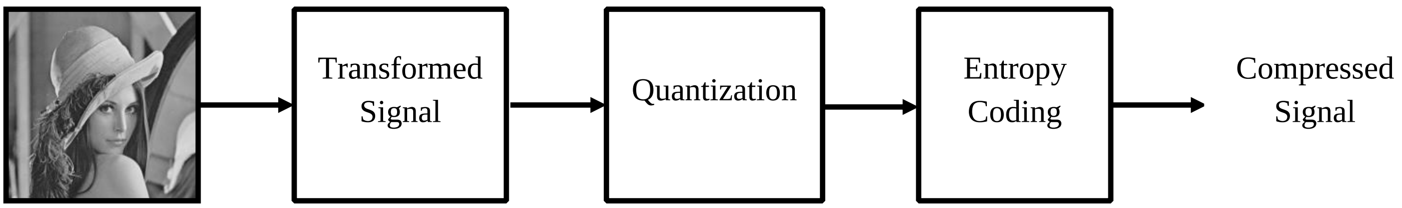

Figure 2.1 Block diagram of lossy compression.

The three stages in lossy compression are:

i. Transform: is the first stage in lossy compression and is used to eliminate the inter-pixel redundancy to pack information efficiently [20].
ii. Quantization: is the second stage and used for removing psycho-visual redundancy. The quantization output is a packed information with as few bits as possible [20].
iii. Encoding: is the third stage and used for removing coding redundancy [20].

The compression process is reversible. Figure 2.2 shows a general block diagram of the decompression process.

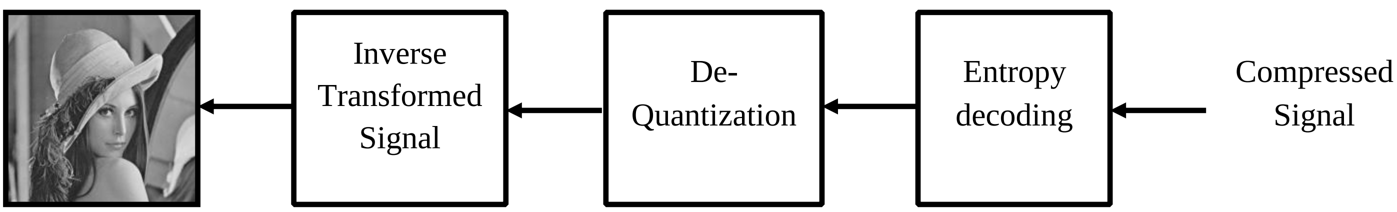

Figure 2.2 The decompression process.

2.2.1 Image Transform

An image is transformed from one domain to a different type of representation, using some well-known transform. Then the transformed values are coded and thus provide greater data compression [21]. Different types of linear transforms are introduced in the literature such as the Discrete Fourier Transforms (DFT), Discrete Cosine Transforms (DCT), Discrete Wavelet Transform (DWT) and the Stockwell (S) Transform [17]. Figure 2.3 presents the original grayscale test image of Lena and the amplitude spectrum of its discrete orthonormal S transform (DOST).

Figure 2.3 Lena grayscale test image (left) and its DOST transform (right).

The transform operation by itself does not achieve any compression. It aims at decorrelating the original data and compacting a large fraction of the signal energy into a relatively small set of transform coefficients [21]. In this way, many coefficients can be discarded after quantization and prior to encoding. The main idea of transform coding is that, if the transformed signal is less correlated compared with the original signal, then quantizing and encoding the transformed signal may lead to data compression [21]. That means the higher the correlation among the image pixels, the better is the compression ratio that is achieved. After the image transformation, the quantizing and encoding processes complete the compression step. At the receiving or decompression stage, decoding and dequantizing allow the compressed image data to be transformed back to its original form so that we can have the reconstructed image.

As mentioned above image compression has two sides, compression and decompression which are termed in some literatures as encoding and decoding respectively [17] [20] [21]. In the compression step transforming the image from spatial domain to the transformed domain is the first step. After the transform the image is represented by the transform coefficients, usually the number of coefficients is equal to the number of elements (pixels) in the image [21]. During the decompression process, the inverse transform is the last step which reconstructs the image.

There are various transforms being used in the literature for data compression [20]. Some of them are:

i. DCT (Discrete Cosine transform)
ii. DWT (Discrete Wavelet transform)
iii. DFT (Discrete Fourier transform)
iv. DST (Discrete S - transform)

The Fourier transform will be discussed in the next chapter while the Stockwell transform is being introduced. In the next subsections the Discrete Cosine and Discrete Wavelet Transforms are discussed.

2.2.2.1 The Discrete Cosine Transform (DCT)

The Discrete Cosine Transform (DCT) has emerged as the de-facto image transformation in most visual systems in the last decades [22]. The 2D DCT transforms a signal from a spatial representation into a frequency representation without involving complex arithmetic like in the case of the complex Fourier transform [21]. It is used to decorrelate the image data then the transform coefficients can be encoded independently without losing compression efficiency. DCT, however, is poor in frequency localization due to the inadequate basis window [13]. For an input image *h(x,y)* the 2D DCT can be defined as:

$$F(m,n)=\alpha_m\alpha_n\sum_{x=0}^{M-1}\sum_{y=0}^{N-1}h(x,y)\cos\frac{(2x+1)m\pi}{2M}\cos\frac{(2y+1)n\pi}{2N} \quad \ldots\ldots 2.1$$

where m = 0,1,2,…,M−1 and n = 0,1,2,…,N −1.

where $\alpha_m=\begin{cases}\frac{1}{\sqrt{M}}, m=0\\ \sqrt{\frac{2}{M}}, 1\le m\le M-1\end{cases}$ and $\alpha_n=\begin{cases}\frac{1}{\sqrt{N}}, n=0\\ \sqrt{\frac{2}{N}}, 1\le n\le N-1\end{cases}$

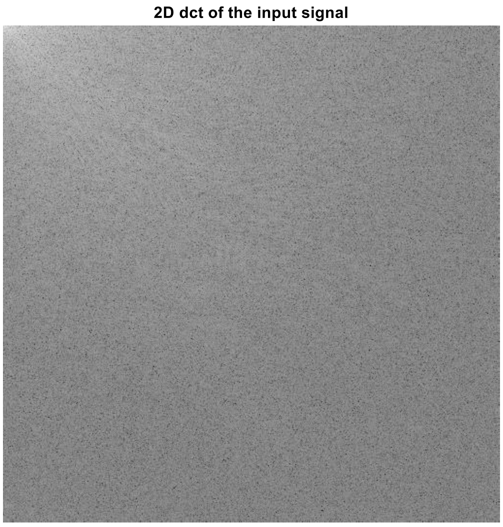

Figure 2.4 DCT of Lena test image.

The 2D inverse DCT is given by:

$$h(x,y) = \sum_{m=0}^{M-1}\sum_{n=0}^{N-1} \alpha_m \alpha_n F(m,n) \cos\frac{(2x+1)m\pi}{2M} \cos\frac{(2y+1)n\pi}{2N} \qquad \text{..........2.2}$$

Below are some useful properties of the DCT [22][23]:

i. Decorrelation: the removal of redundancy between neighboring pixels leads to uncorrelated transform coefficients which can be encoded independently. This is the principal advantage of image transformation. DCT exhibits excellent decorrelation properties.

ii. Separebility: has the principle advantage that the transformed signal (*F (m,n)*) can be computed in two steps by successive 1-D operations on rows and columns of an image and the DCT is a separable transform.

$$F(m,n) = \alpha_m \alpha_n \sum_{x=0}^{M-1} \cos\frac{(2x+1)m\pi}{2M} \sum_{y=0}^{N-1} h(x,y) \cos\frac{(2y+1)n\pi}{2N} \qquad \text{..........2.3}$$

iii. Symmetry: the row and column operations in the above equation reveal that these operations are functionally identical.

iv. Orthogonality: the inverse transformation matrix is equal to its transpose. This property renders some reduction in the pre-computation complexity.

2.2.2.1.2 Limitations of the DCT

For higher compression ratio, the DCT has the following two limitations.

i. Blocking artifacts: It is a distortion that appears due to heavy compression and appears as abnormally large pixel blocks [21].

ii. False contouring**:** It occurs when smoothly graded area of an image is distorted by deviation that looks like a contour map for specific images having gradually shaded areas [21]. This is due to heavy quantization.

JPEG image compression uses DCT as a transform coding. The acronym JPEG stands for Joint Photographic Experts Group. This is a group of image processing experts nominated by national standard bodies and major companies to work to produce standards for continuous tone image coding.

2.2.2.2 The Wavelet Transform (WT)

Smaller size and low contrast images are examined at high resolution but if the images are large in size and with high contrast a coarse view is all that is required [20]. The question is what if an image is composed of both cases, i.e. high and low contrast with large and small in size? This question leads as to the concept of multiresolution processing [20].

The multiresolution concept is designed to represent signals, where a single event will be decomposed into finer and finer details [21]. A signal is represented by a coarse approximation and finer details. The coarse and the detail subspaces are orthogonal to each other and by applying successive approximation recursively the space of the input signal can be spanned by spaces of successive details at all resolutions [21]. Multiresolution analysis enables detecting patterns that are not visible in the raw data. Wavelets can obtain multiscale variance estimates of a signal or measure the multiscale correlation between two signals. Wavelets produce a natural multi resolution of every image.

The term wavelet means a small wave [23] [24]. The smallness refers to the condition that this (window) function is of finite length (compactly supported) and the wave refers to the condition that this function is oscillatory [23]. Wavelets are adjustable and hence can be designed to suit the individual applications [21]. In the 1D case, the main purpose of the wavelet transform is to change the signal from time domain to joint time-frequency domain while for 2D signals/images wavelets allow transformation from space domain to joint space-wavenumber (spatial frequency) domain which makes better compression results [24].

For an input signal *h(t)*, the 1D continuous wavelet transform is given by:

$$WT(s,\tau) = \frac{1}{\sqrt{|s|}} \int_{-\infty}^{\infty} h(t)\omega\left(\frac{t-\tau}{s}\right)dt \quad \ldots\ldots 2.4$$

where ω is the wavelet function, s is the scale factor (or dilation parameter) that is the inverse of the frequency; and τ is the translation variable with the appropriate choice of wavelet function.

Two wavelet functions commonly used in wavelet analysis are the Mexican Hat wavelet and the Morlet wavelet [24][34]. The Mexican Hat wavelet is defined as the second derivative of the Gaussian function which is given by:

$$\omega(t) = \frac{1}{\sqrt{2\pi}\sigma^3} e^{\frac{-t^2}{2\sigma^2}} \left(\frac{t^2}{\sigma^2} - 1\right) \quad \ldots\ldots 2.5$$

The Morlet wavelet is composed of a complex exponential multiplied by a Gaussian window. This wavelet is believed to be closely related to the human perception of signals [33][35]. It is given by:

$$m(t) = e^{iat} e^{\frac{-t^2}{2\sigma}} \quad \ldots 2.6$$

The simplest and the oldest wavelet function is the Haar wavelet and is given by (assuming time is normalized between 0 and 1):

$$\omega(t) = \begin{cases} 1, \ 0 \le t < \frac{1}{2} \\ -1, \ \frac{1}{2} \le t < 1 \\ 0, \text{otherwise} \end{cases} \quad \ldots 2.7$$

For reconstruction of the original time series, the inverse WT is used which in principle is given by the double integral:

$$h(t) = \frac{1}{C_\omega^2} \int_s \int_\tau WT(s,\tau) \frac{1}{s^2} \omega\left(\frac{t-\tau}{s}\right) d\tau ds \quad \ldots 2.8$$

The above is valid provided that the admissibility condition given below is satisfied.

$$C_\omega = \left(2\pi \int_{-\infty}^{\infty} \frac{F(\varepsilon)}{|\varepsilon|} d\varepsilon \right)^{\frac{1}{2}} < \infty \quad \ldots 2.9$$

2.2.2.2.1 The Discrete Wavelet Transform

The discrete wavelet transform (DWT) could be easily understood using successive applications of a pair of lowpass and highpass filters. The set of these filters is called filter bank. It consists of analysis bank and synthesis bank. The analysis bank separates the input signal into frequency bands and the synthesis bank is the inverse of the analysis bank. Figure 2.5 and Figure 2.6 describe the two filters. It is known that the lowpass filter preserves the low frequencies of a signal while attenuating the high frequencies, and the result is a blurred version of the original signal. The highpass filter preserves the high frequencies in a signal and attenuates the low frequencies. The filtered samples that are outputted from the forward DWT are referred to as wavelet coefficients [29] [21].

The total number of wavelet coefficients is the same as the number of original signal samples. The reconstruction of a signal from the wavelet coefficients at the decoder is performed with another pair of lowpass and highpass filters [29]. The filter pair is designed in such a manner that after downsampling the output of each filter by a factor of two, the original signal can still be completely recovered from the remaining samples in the absence of any quantization errors [29].

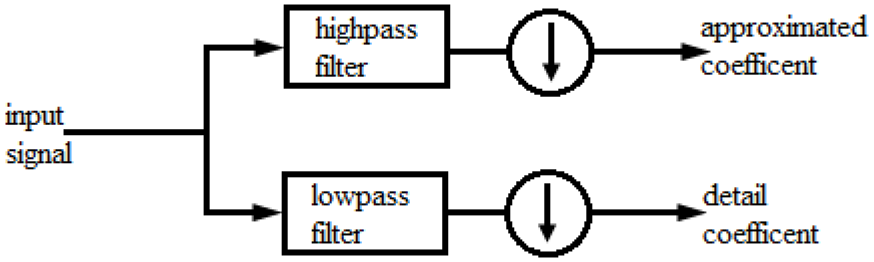

Figure 2.5 Analysis filter bank.

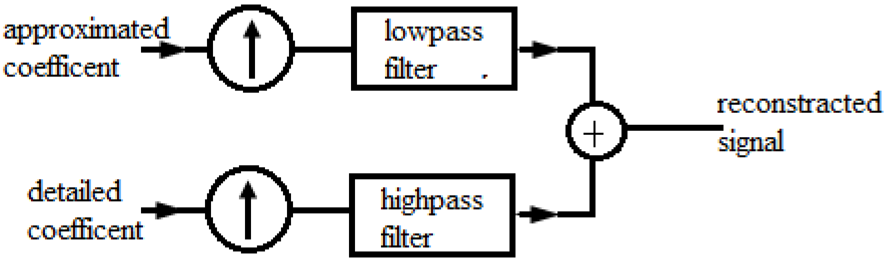

Figure 2.6 Synthesis filter bank.

The 1D DWT can be easily extended to two dimensions (2D) by applying the filter bank in a separable manner (as shown in Figure 2.7 and Figure 2.8). At each level of the wavelet decomposition, each row of a 2D image is first transformed using a 1D horizontal analysis filter bank. The same filter bank is then applied vertically to each column of the filtered and subsampled data.

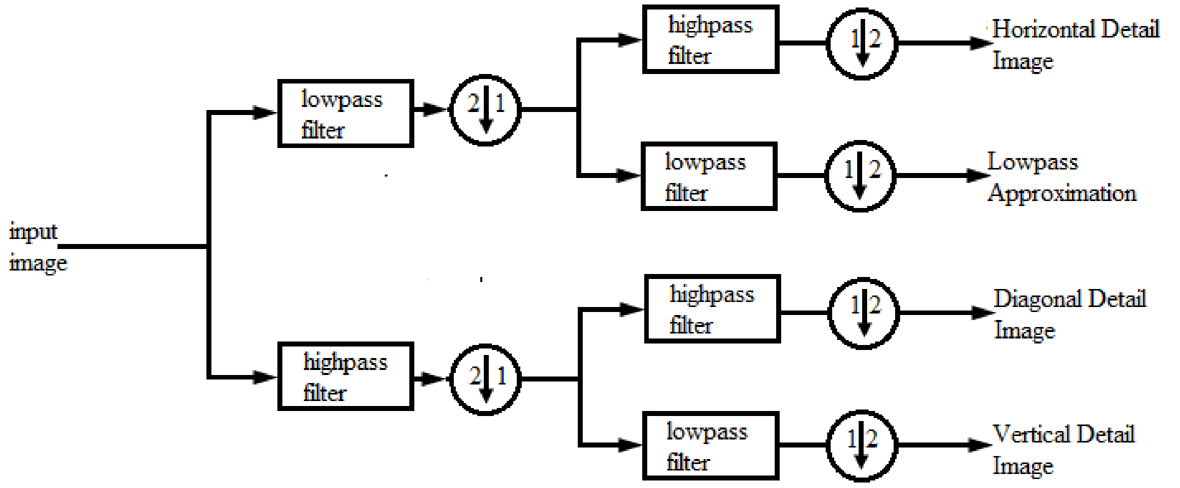

Figure 2.7 2D analysis filter bank.

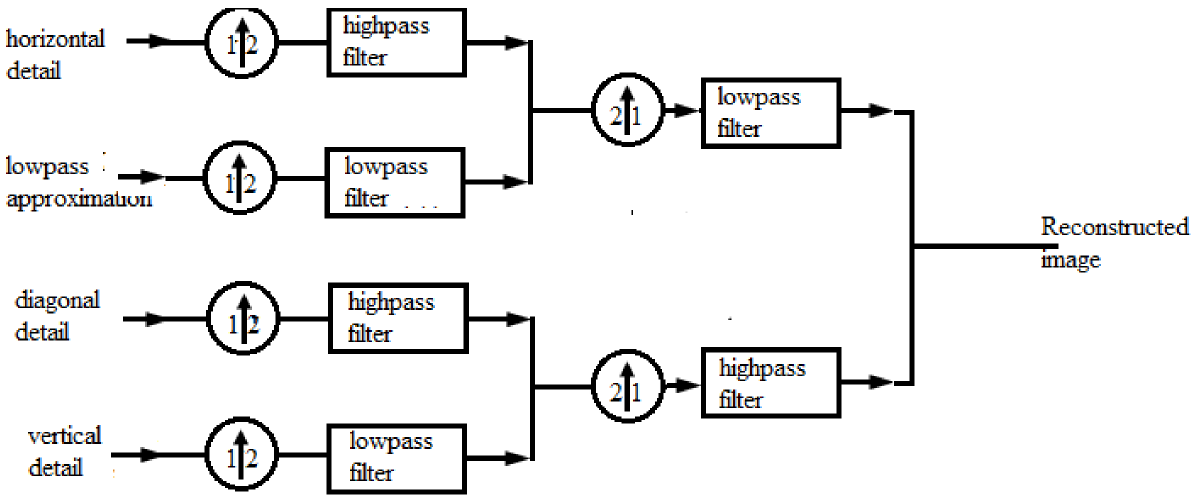

Figure 2.8 2D synthesis filter bank.

The output is obtained in set of four coefficients LL, HL, LH and HH. The first alphabet represents the transform in row whereas the second alphabet represents transform in column. The alphabet L means low pass signal and H means high pass signal. LH signal is a low pass signal in row and a high pass in column. Hence, LH signal contain horizontal elements. Similarly, HL and HH contain vertical and diagonal elements, respectively. Figure 2.9 shows the wavelet transformed coefficients of Lena test image.

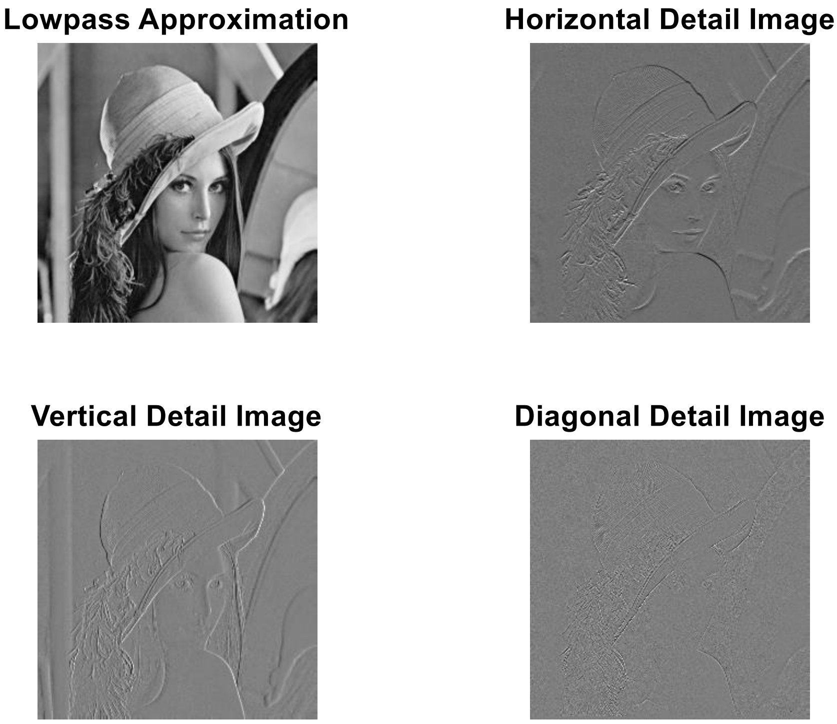

*Figure 2.9 W*avelet transformed coefficents computed on Lena test image.

2.2.2 Quantizer

Quantizer is a key component in the transform compression framework that introduces non-linearity in the system. It maps the transformed digital image to a discrete set of levels [23]. In the mapping process, the quantization introduces an error and therefore it is used in a lossy compression technique. The original transformed signal could not be recovered in the inverse quantization process as there is round off error. A good quantizer is one which represents the original signal with minimum loss or distortion. Based on their working principles, quantizers are of three major types which are:

i. Scalar Quantization**:** is the simplest quantization scheme. It can be described as a function Q that maps each element in a subset of the real line to a particular value. For a given transformed coefficient *x*, the quantizer produces a signed integer *q* given by:

$q = Q(x)$ ……………………………………………………………………………………………….2.10

The quantization index *q* indicates the interval in which *x* lies [30]. This is done in the encoding process.
In the decoding process, if we assume q be given, therefore the decoder produces an estimate of *x* as

$\hat{x} = \overline{Q^{-1}}(q)$ ……………………………………………………………………………………………….2.11

Scalar quantization produces lossy compression but it makes easy to control the trade-off between compression performance and the amount of data loss [23].

ii. Vector Quantization: here the input samples are clubbed together in groups called vectors and then processed to give the output. If each data symbol is a vector, then vector quantization converts a data symbol to another vector [23]. The idea of representing groups of samples rather than individual samples is the main concept of vector quantization. Vector quantization is based on the fact that adjacent data symbols in image and audio files are correlated [23].

Shannon first showed that vector quantization would result in a lower bit rate than scalar quantization. But vector quantization suffers from a lack of generality, since the codebook must be trained on some set of initial images. As a result, the design of the codebook will directly affect the bit rate and distortion of the compression [31].

iii. Predictive Quantization: The quantization of the difference between the predicted value and the past samples is called predictive quantization.

2.2.3 Entropy Coding

Entropy coding is used after quantization of the transformed values for additional compression. It is a lossless compression and is also reversible. In the entropy encoding, the idea is to find a reversible mapping to the quantized values such that the average number of bits or symbols is minimized [21]. Entropy represents the minimum size of dataset necessary to convey a particular amount of information. Huffman coding, LZ (Lempel-Ziv) coding and arithmetic coding are the commonly used entropy coding schemes [33]. Below, Huffman coding and arithmetic coding are briefly discussed.

i. Huffman coding: Huffman coding technique is based on the following two observations regarding optimum prefix codes.
    a. The more frequently occurring symbols can be allocated with shorter code words than the less frequently occurring symbols.
    b. The two least frequently occurring symbols will have code words of the same length, and they differ only in the least significant bit.

  Average length of these codes is close to entropy of the source [33]. Therefore, it utilizes a variable length code in which short code words are assigned to more common values or symbols in the data, and longer code words are assigned to less frequently occurring values.

ii. Arithmetic coding: Arithmetic coding is a common algorithm used in both lossless and lossy data compression algorithm. It is an entropy encoding technique in which the frequently seen symbols are encoded with fewer bits than rarely seen symbols [12]. The sequence of input symbols is represented by an interval of real numbers between 0 and 1. Basically, it divides the intervals between 0 and 1 into a number of smaller intervals corresponding to the probabilities of the input signal. Then the first input symbol selects an interval, which is further divided into smaller intervals. The next input symbol selects one of these intervals, and the procedure is repeated. As a result, the selected interval narrows with every symbol, and in the end, any number inside the final interval can be used to represent the message. The longer the message, the smaller the interval to represent. More probable symbols reduce the interval less than the less probable symbols and hence add fewer bits in the encoded message [33]. Therefore, the coding result can reach to Shannon's entropy limit (Shannon's theorem is widely discussed in the compression literature) for a sufficiently large sequence of input symbols as long as the statistics are accurate [33].

The Huffman coding in the JPEG standard has a very simple algorithm while the more complex arithmetic coding in the JPEG-2000 standard achieves 5 to 10 percent more compression rate [32]. Generally, arithmetic coding offers superior efficiency and more flexibility compared to Huffman coding [33].

If we consider for example JPEG-2000 technique for compression of medical images, it uses the algorithm based on wavelet transform image decomposition and arithmetic coding [3]. This method has relatively low compression ratio and compression speed, but it has higher quality final image. In the current thesis work it was intended to modify JPEG-2000 technique by replacing the wavelet transform and its coding scheme targeting increased compression ratio and compression speed by maintaining the quality of the final image.

2.3 Lossless Image Compression

In lossless compression, also called error-free compression, the exact replica of the original image can be retrieved by the decompression process from the compressed image [20]. It is also known as entropy coding as it uses decomposition techniques to minimize loopholes [37]. If the deviation between the original data and the decompressed image is not acceptable, we use lossless image compression as it has no loss of information. It generally uses two independent oppressions which is reducing interpixel redundancy and eliminating coding redundancy [20].

The advantage of lossless image compression technique is that it maintains the original quality. But the problem is that the compression ratio of this technique is usually minimum. Lossless compression schemes normally provide a compression ratio of 2 to 10 [20]. Lossless image compression is categorized as:

i. Entropy Based Encoding: In this compression process the algorithm first counts the frequency of occurrence of each pixel in the image. Then the compression technique replaces the pixels with the algorithm generated pixel. These generated pixels are fixed for a certain pixel of the original image; and doesn't depend on the content of the image. The length of the generated pixels is variable and it varies on the frequency of the certain pixel in the original image [42].
ii. Dictionary Based Encoding: This encoding process is also known as substitution encoding. In this process the encoder maintains a data structure known as 'Dictionary'. This is basically a collection of strings. The encoder matches the substrings chosen from the original pixel and finds it in the

dictionary; if a successful match is found then the pixels is replaced by a reference to the dictionary in the encoded file [42].

Below are some of the lossless compression techniques which are briefly discussed. Huffman and Arithmetic coding have already been discussed in the previous section.

2.3.1 LZW coding

Lempel, Ziv and Welch (LZW) compression is simple dictionary based compression algorithm named after the algorithm developers, Abraham Lempel, Jakob Ziv and Terry Welch [38][39]. It reduces interpixel redundancy. LZW compression is always used in GIF image files, and offered as an option in TIFF and PostScript [38]. It replaces sequence of data or pixel with single codes and creates dynamic dictionary of codes without doing any analysis of the incoming data or pixel [39, 40]. It keeps on updating the table by adding every new string of data or pixel it reads. The data compression occurs on the single code. It starts with an initial model, then read each part of data or pixel, and at last it updates the model and encode the data or pixel. The code generated by LZW can be of random length. The default size of table is 256 to hold pixel values from 0 to 255 for 8 bits [20] [40]. The table can be extended up to 4095 based on new pattern strings it forms in the process [40]. It was the algorithm of the widely used UNIX file compression, and is used in the GIF image format. LZW compression became the first widely used universal image compression method on computers.

2.3.2 Run Length Encoding

It is a lossless compression technique of input data based on sequence of identical values. Run length encoding is mostly used on data that contains many runs of data, sequences in which the same data value occurs in many consecutive data elements [41]. Icons, line drawings which are a simple graphic image are good examples as they have many runs of data or a sequence of identical values. In this technique of lossless compression, the longest sequence of the same symbol is replaced by shorter sequence. By replacing these repeated byte sequences with the number of occurrences, a reduction of data can be achieved.

Run length encoding technique is not useful with files that don't have many runs as it could greatly increase the file size [42]. Although JPEG uses it quite effectively on the coefficients that remain after transforming and quantizing image blocks, it is not well suited for continuous tone images like medical images, or photographs [38].

2.3.3 Area Coding

Area coding is also known as two-dimensional run length coding as it is enhanced method of run length coding [20]. It focuses on two dimensional characteristics of an image. The whole image is divided into blocks of size m x n pixels, which are classified as blocks having only white pixels, blocks having only black pixels or blocks with mixed intensity. This approach takes advantage of the anticipated structural patterns of the image to be compressed. The most frequently occurring category is assigned by one-bit code word 0 and the other categories are assigned with two bit codes 10 and 11 [39]. Compression is achieved because the mn bits that used to represent one area is replaced by one bit or two-bit code word. Relative address coding (RAC) is one of the better-known results which is based on the principle of tracking the binary transition that begin and end each black and white run. Area coding is highly effective and can give better compression ratio but it has certain limitations in that it uses non-linear method which is inapplicable in hardware [37].

In general, we can use lossless and lossy techniques for image compression. They both have merits and demerits. In lossless compression, we can achieve compression without any loss of information. But the compression ratio is minimum. In case of lossy compression technique, we can achieve a better compression ratio but there is acceptable loss of information.

Chapter Three

The Stockwell (S) Transform

3.1 Introduction

The Fourier transform is commonly used to decompose a signal into its frequency components in signal and image processing [23]. Fourier transform of a one-dimensional function is defined as:

$$H(f) = F\{h(t)\} = \int_{-\infty}^{\infty} h(t)e^{-i2\pi ft}dt \quad \text{.......................................} 3.1$$

The inverse Fourier transform (IFT) of *H(f)* is defined as:

$$h(t) = \int_{-\infty}^{\infty} H(f)e^{i2\pi ft}df \quad \text{.......................................} 3.2$$

Due to the perfect localization of the Fourier transform in the frequency domain, the information in time (or space) domain has been entirely smeared into all Fourier coefficients. Tiny deviations of the Fourier coefficients could cause huge deviations of the time component. That is to say, a function in real world can never be both band-limited (compact in Fourier domain) and time-limited (compact in time domain) [23]. In order to resolve this global issue one may use the short-time Fourier transform (STFT) [23]. The STFT is given by:

$$STFT\{h(t)\} = G(\tau, f) = \int_{-\infty}^{\infty} h(t)\omega(t-\tau)e^{-i2\pi ft}dt \quad \text{.......................................} 3.3$$

And the inverse STFT is:

$$h(t) = \frac{1}{\omega(0)}\int_{-\infty}^{\infty} G(\tau, f)e^{i2\pi ft}df = \frac{1}{\omega(0)}F^{-1}(G(\tau, f)) \quad \text{.......................................} 3.4$$

where τ is a translation variable that allows the window to translate in time. The width of the windowing function relates to how the signal is represented, it determines whether there is good frequency resolution or good time resolution that means STFT has a fixed resolution. A wide window gives better frequency resolution but poor time resolution and narrower window gives good time resolution but poor frequency resolution. This leads to multiresolution analysis [23][26]. The wavelet transforms successfully overcome the shortcomings of the STFT [23].

The continuous wavelet transform for a continuous-domain input is given as:

$$W(\tau, s) = \frac{1}{\sqrt{s}} \int_{-\infty}^{\infty} h(t)\psi\left(\frac{t-\tau}{s}\right)dt \quad \text{...3.5}$$

where τ is a translation variable while s is a scaling parameter.

If an image is decomposed by wavelets, the overlap in the frequency domain becomes non-avoidable. Even though the term "scale" can be approximately interpreted as "frequency" due to its ability in adjusting the size of the basis function, there is no straightforward way to turn this scale information into proper frequency information [23]. In response to this restriction, the Stockwell transform was published [23].

The Stockwell (S) transform was first proposed in 1996 by R. G. Stockwell which gives a full time-frequency decomposition of a signal [23][24][25][26][27]. It maintains the absolutely-referenced frequency and phase information.

3.2 The 1-D Stockwell Transform

The Stockwell transform of an input signal is defined as the Fourier transform (FT) of the product between the input signal and a Gaussian window function [23][25]. It is based on the continuous wavelet transform, and the STFT [26]. Combining these two transforms, the 1D S transform is given by:

$$S(\tau, f) = S\{h(t)\} = \int_{-\infty}^{\infty} h(t)\frac{|f|}{\sqrt{2\pi}} e^{-\frac{(\tau-t)^2 f^2}{2}} e^{-i2\pi ft} dt \quad \text{...3.6}$$

S (τ, f) decomposes the input signal *h(t)* into temporal (τ) and frequency (*f*) components. The value of τ represents the center of the window function, and thus, by picking all possible values for τ, the S transform coefficients will cover the whole temporal axis and create full resolutions for each designated frequency [23]. Different values of *f* adjust the sizes of the Gaussian window over the temporal axis to realize multiresolution over different frequencies. That is higher resolution on higher frequencies and lower resolution on lower frequencies. Therefore, for different *f* values there will be different resolutions [23]. As opposed to the wavelet transform, the kernel of the S transform is not shifted in time. Only the modulating window (Gaussian) is shifted. Therefore, the phase of the signal does not change with respect to the origin as it does for the wavelet transform [26]. Stockwell calls this phase “absolutely referenced", because at t = 0, the phase of the time-frequency signal is zero [26]. Absolutely-referenced phase information allows the comparison of phases derived from similar time series for correlation analysis [23].

Because the Stockwell coefficients $S(\tau, f)$ are complex, formula 3.6 can be generalized as:

$$S(\tau, f) = A(\tau, f)e^{i\Phi(\tau, f)} \quad \text{……… 3.7}$$

where $A(\tau, f)$ is the “amplitude S-spectrum” and $\Phi(\tau, f)$ is the “phase S-spectrum” which allows the definition of a broadband generalization of instantaneous frequency.

Using the convolution theorem in the Fourier space, the S transform can also be written as:

$$S(\tau, f) = \int_{-\infty}^{\infty} F(\alpha + f)e^{\frac{-2\pi^2\alpha^2}{f^2}} e^{i2\pi\alpha\tau} d\alpha \quad \text{……… 3.8}$$

where $F(\alpha + f)$ is the Fourier transform of $h(t)e^{-i2\pi ft}$.

This allows us to use the Fast Fourier Transform (FFT) while computing the S-transform [26]. The relation between $S(\tau, f)$ and the Fourier transform of $h(t)$ is expressed as [23][27]:

$$H(f) = \int_{-\infty}^{\infty} S(\tau, f)d\tau \quad \text{……… 3.9}$$

where $H(f)$ is the Fourier transform of $h(t)$.

The original function $h(t)$ can be recovered by calculating the inverse Fourier transform of $H(f)$ as [23][27]:

$$h(t) = F^{-1}\{H(f)\} = \int_{-\infty}^{\infty} \left\{ \int_{-\infty}^{\infty} S(\tau, f)d\tau \right\} e^{i2\pi ft} df \quad \text{……… 3.10}$$

For an input $h(m)$, $m = 0,1,\ldots,N-1$, the discrete Stockwell transform (DST) of the input can be defined as:

$$S(j,n) = \sum_{m=0}^{N-1} H(m+n)e^{\frac{-2\pi^2 m^2}{n^2}} e^{\frac{i2\pi mj}{N}} \quad \text{……… 3.11}$$

where $j = 0,1,\ldots,N-1$.

For a fixed value of j, the DST coefficients for different n can be regarded as the inverse Fourier transform of the term $H(m+n)e^{\frac{-2\pi^2 m^2}{n^2}}$.

3.3 The 2-D Stockwell Transform

For a 2-D continuous-domain function $h(x,y)$, the 2-D S transform is defined with a 2-D Gaussian modulate of cosinusoidal functions as:

$$S(X,Y,k_x,k_y) = \int_{-\infty}^{\infty}\int_{-\infty}^{\infty} h(x,y)\frac{|k_x||k_y|}{2\pi} e^{-\frac{(X-x)^2 k_x^2 + (Y-y)^2 k_y^2}{2}} e^{-i2\pi(k_x x + k_y y)} dxdy \quad \ldots\ldots\ldots\ldots\ldots 3.12$$

The Gaussian kernel changes shape with respect to spatial frequencies k_x and k_y in the x and y directions respectively.

Similar to the 2-D Fourier transform, the 2-D S transform is a separable transform over different dimensions [23], therefore, calculation can be pursued first over one dimension and then over the other dimension. Using the 2D convolution theorem in the Fourier space, the 2-D S transform can be written as:

$$S(X,Y,k_x,k_y) = \int_{-\infty}^{\infty}\int_{-\infty}^{\infty} F(\alpha + k_x, \beta + k_y) e^{\frac{-2\pi^2\alpha^2}{k_x^2}} e^{\frac{-2\pi^2\beta^2}{k_y^2}} e^{i2\pi(\alpha X + \beta Y)} d\alpha d\beta \quad \ldots\ldots\ldots\ldots\ldots\ldots\ldots\ldots 3.13$$

Therefore, we can use 2-D FFT to compute the 2-D S transform [26].

Integration of $S(X, Y, k_x, k_y)$ over the variables x and y gives the 2-D Fourier spectrum

$$H(k_x,k_y) = \int_{-\infty}^{\infty}\int_{-\infty}^{\infty} S(X,Y,k_x,k_y) dXdY \quad \ldots\ldots\ldots\ldots\ldots\ldots\ldots\ldots\ldots\ldots\ldots\ldots 3.14$$

Then the 2-D inverse Fourier transform can be applied to $H(k_x, k_y)$ to recover the original function.

For an input 2-D signal (image), the 2-D Stockwell transform is a complex function of x, y, k_x and k_y which gives convenience and the freedom to manipulate data over spatial and frequency domains. The transformed data has four-dimensional data set which gives a big challenge in possessing, analyzing and visualizing the coefficients.

Therefore, we only analyze, process, compute or store relevant components of the $S(x, y, k_x, k_y)$ [23]. We will describe one of the strategies to deal with this challenge later in this chapter.

The discrete 2-D Stockwell coefficients of an image $h(p, q)$can be expressed explicitly as:

$$S(p,q,n,m)=\sum_{n'=0}^{N-1}\sum_{m'=0}^{M-1}H(n'+n,m'+m)e^{-\frac{2\pi^2 n'^2}{n^2}}e^{\frac{i2\pi n'p}{N}}e^{-\frac{2\pi^2 m'^2}{m^2}}e^{\frac{i2\pi m'q}{M}} \quad \ldots\ldots 3.15$$

where $p = 0,1,\ldots,N-1$ and $q = 0,1,\ldots,M-1$.

It is shown in the continues S transform that integration of $S(x, y, k_x, k_y)$ over the variables x and y gives the 2-D Fourier spectrum. Similarly summation of $S(p,q,n,m)$ over the variables p and q gives the 2-D discreet Fourier spectrum.

$$\frac{1}{M}\sum_{q=0}^{M-1}\frac{1}{N}\sum_{p=0}^{N-1}S(p,q,n,m)=H(n,m) \quad \ldots\ldots 3.16$$

where $H(n,m)$ are the discrete 2-D Fourier coefficients.

The original image can be reconstructed using:

$$h(p,q)=\left(\frac{1}{M}\right)^2\sum_{q'=0}^{M-1}\sum_{m=0}^{M-1}\left(\frac{1}{N}\right)^2\sum_{p'=0}^{N-1}\sum_{n=0}^{N-1}S(p',q',n,m)e^{\frac{i2\pi np}{N}}e^{\frac{i2\pi mq}{M}} \quad \ldots\ldots 3.17$$

3.4 Properties of the S transform

As the S transform is derived from the Fourier transform, it shares some similar properties. The following are some properties of the S transform

i. Linearity: Assuming h(t), g(t) ∈**L**1(R) and **a, b** are arbitrarily complex numbers, the linear property holds as:

$$S\{ah(t)+bg(t)\}=aS\{h(t)\}+bS\{g(t)\} \quad \ldots\ldots 3.18$$

That implies that for a data with additive noise, $S\{data\}=S\{signal\}+S\{noise\}$.

Linearity is particularly important for the case of additive noise [23][26].

ii. Symmetry: The S transform of a real function is a conjugate-symmetric function so that half the calculation can be saved in decomposition [23].

iii. Modulation: Shifting a function introduces into its spectrum a phase shift that is linear with frequency besides the shifting on the coefficients itself [23].

$$S\{h(t-t_0)\}=e^{-i2\pi f t_0}S(\tau-t_0,f) \quad \ldots\ldots 3.19$$

iv. Scaling: Narrowing a function with a scale ***a*** will broaden its ST coefficients in the scale of ***1/a***, and vice versa.

v. The Absolutely Referenced Phase Information: by not translating the oscillatory exponential kernel, the ST localizes the real and the imaginary components of the spectrum independently, localizing the phase spectrum as well as the amplitude spectrum.

3.5 Discrete Orthonormal Stockwell Transform

The Stockwell transform is an overcomplete representation. For a signal of length N, there are N^2 Stockwell coefficients and therefore the computing of all N^2 coefficients of the Stockwell transform has computational complexity. If the dimension for the input signal is higher, the computational complexity is also higher. The ST gets exponentially more expensive for higher-dimensional signals [23][28]. As discussed earlier in this chapter, we need more efficiency to pursue this spatial-frequency decomposition. The Discrete Orthonormal Stockwell Transform (DOST) is the best solution to reduce the computational cost without changing its multiresolution nature and the absolutely-referenced frequency and phase information.

The DOST is a pared-down version of the fully redundant Stockwell transform [23][26][28]. The Nyquist criterion indicates that low frequency band and high frequency band have very different sampling requirements. Lower frequencies have longer periods and high frequencies have smaller periods. So lower frequencies have lower sampling rates and higher frequencies have higher sampling rates. Hence, the DOST subsamples the low frequencies and takes the advantage of this sample spacing paradigm, and distributes its coefficients accordingly for higher frequencies. It does so by constructing a set of N orthogonal unit-length basis vectors, each of which targets a particular region in the time-frequency domain [23]. Which region is dictated by a set of parameters: ν specifies the center of each frequency band (voice), β is the width of that band, and τ specifies the location in time. Using these parameters, the kth basis vector is defined as [23][28].

$$D[k][\nu,\beta,\tau] = \frac{1}{\sqrt{\beta}} \sum_{f=\nu-\beta/2}^{\nu+\beta/2-1} \left(e^{-i2\pi \frac{k}{N} f} \right) \left(e^{i2\pi \frac{\tau}{\beta} f} \right) \left(e^{-i\pi\tau} \right) \quad \text{.........3.19}$$

for k = 0, 1,…,N − 1, which can be summed analytically to:

$$D[k][\nu,\beta,\tau] = ie^{-i\pi\tau \frac{e^{-i2\alpha\left(\nu-\beta/2-1/2\right)} - e^{-i2\alpha\left(\nu+\beta/2-1/2\right)}}{2\sqrt{\beta}\sin\alpha}} \quad \text{.........3.20}$$

where $\alpha = \pi\left(k/N - \tau/\beta \right)$ is the center of the temporal window. Figure 3.1 presents the DOST computed on Lena test image while Figures 3.2 and 3.3 presents DOSTs computed on sample CT and MRI images respectively.

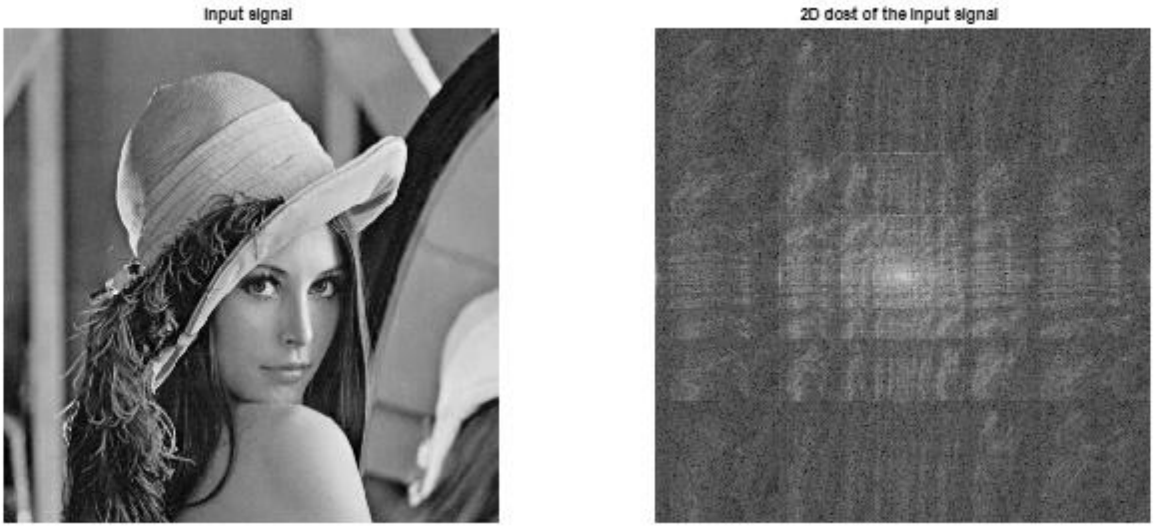

Figure 3.1 DOST of Lena.

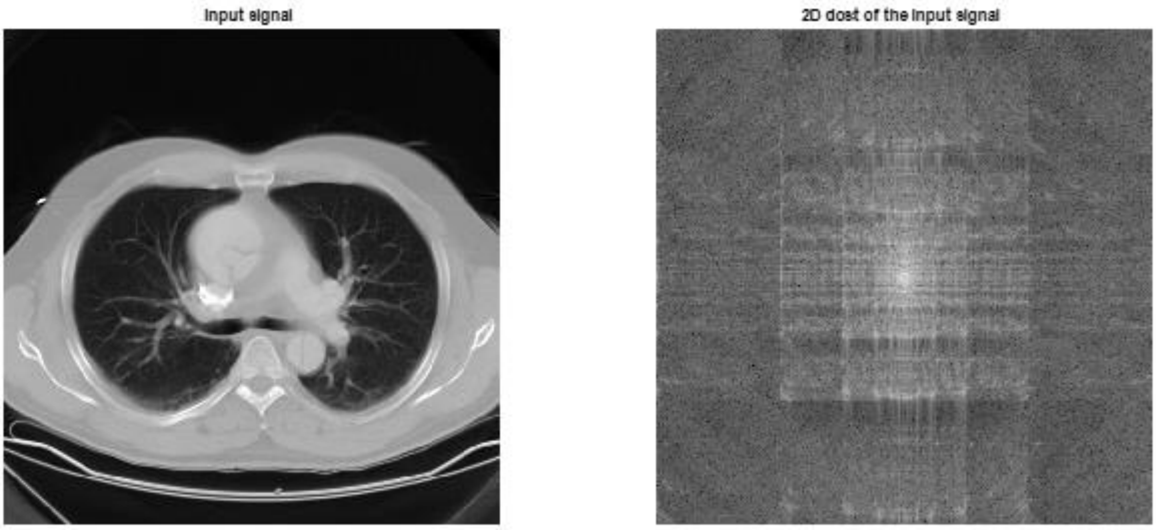

Figure 3.2 DOST of a CT scan image.

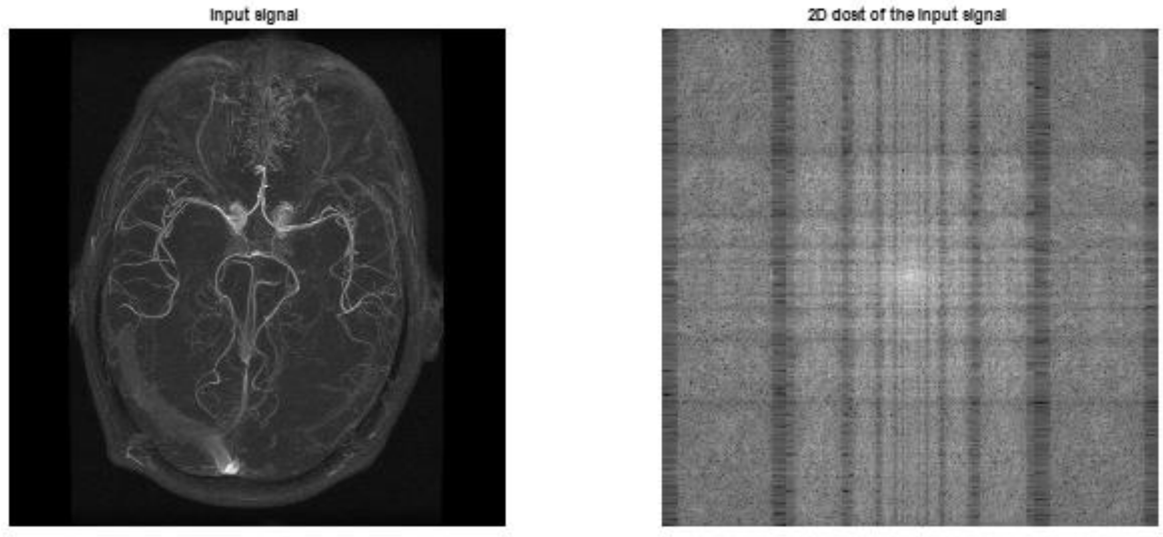

Figure 3.3 DOST of an MRI image.

3.6 ST vs WT

Even though the ST and the WT share some similar properties, they are different kinds of transforms due to the following reasons:

i. In the CWT, the integral of the mother wavelets function is zero and the integral of the scaling function is one. However, the integral of the ST basis function, which is the multiplication between the Fourier basis and the Gaussian window, has no fixed value [23].
ii. In the CWT, only the scale information can be expected with a modulated phase information. However, in the ST, a direct relation exists between the ST coefficients and the FT coefficients, and the exact frequency and phase information can be achieved without reconstructing the images.

Overall, since the inception of the ST in 1996, its special advantages (multiresolution ability, keeping absolutely-referenced frequency and phase information) has helped the ST outperform the STFT and the WT in various fields [23].

Chapter Four

S Transform Based Medical Image Compression

4.1 Methods

The S transform based medical image compression scheme developed in this thesis uses JPEG2000 as a bench mark. JPEG 2000 compression is developed based on the wavelet transform. The comparison between the wavelet and S transforms has been discussed in Chapter Three in which the S transform outperforms the wavelet transform in some useful aspects. Therefore, in the proposed scheme the wavelet transform is replaced by the S transform. As the two-dimensional S transform is fully redundant and has high dimensional data set which increases the storage and computing efficiency, the two-dimensional DOST has been used. The DOST had been discussed in Chapter Three. The rest of the image compression blocks are similar with JPEG2000 image compression scheme. The general block diagram for S transform-based image compression (encoding stage) is shown in Figure 4.1 below.

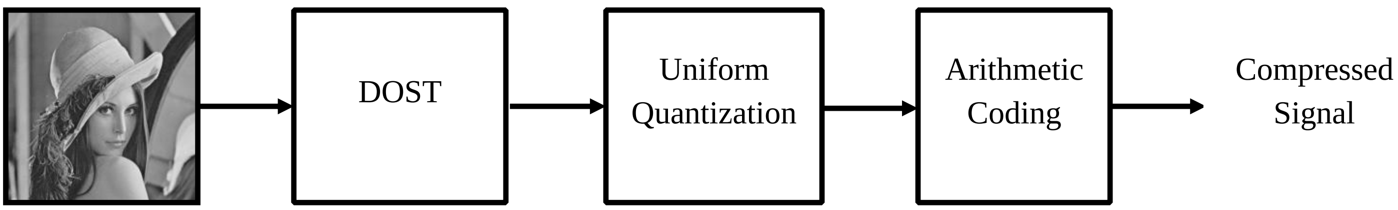

Figure 4.1 Block diagram of the encoding process by the proposed compression scheme.

As seen in the figure, the first step in the image compression is transforming the image using DOST which gives convenience and the freedom to manipulate data over spatial and frequency domains. The next step is quantization. Quantization is used in lossy image compression but it gives good image compression ratio [30]. We used uniform quantization index as in JPEG2000 which is one of the soft quantization schemes which has minimum data loss. Uniform quantization index is given as:

$$q_b(u,v) = sign(y_b(u,v)) \left\lfloor \frac{|y_b(u,v)|}{\Delta_b} \right\rfloor \quad \ldots\ldots 4.1$$

where, $y_b(u,v)$ is the DOST coefficient in a sub-band b, The step-size Δ_b is represented with a total of two bytes, an 11-bit mantissa μ_b, and a 5-bit exponent ε_b, according to the following relationship: $\Delta_b = 2^{R_b - \varepsilon_b}\left(1 + \frac{\mu_b}{2^{11}}\right)$ and R_b is the number of bits representing the nominal dynamic range of the sub-band b.

After the quantization step, the quantized coefficients are arithmetically coded. EBCOT (Embedded Block Coding with Optimal Truncation Points) contextual coder has been used in this regard similar to the step used in the JPEG2000 implementation [32] [36]. This is the last step in the compression process.

The decompressing stage is the complete inverse of the compression step. The compressed code streams are first arithmetically decoded. The arithmetic coding and decoding had been discussed in Chapter Two. As discussed earlier, the two most used entropy coding algorithms are arithmetic coding and Huffman coding. As arithmetic coding offers superior efficiency and more flexibility compared to Huffman coding, arithmetic coding has been adopted in this thesis. After the arithmetic decoding, the next step is dequantizing. The dequantizing is done by using the formula below:

$$Rq_b(u,v) = \begin{cases} (q_b(u,v) + \gamma)\Delta_b\,, & if\ q_b(u,v) > 0 \\ (q_b(u,v) - \gamma)\Delta_b\,, & \text{if } q_b(u,v) < 0 \\ 0\,, & \text{otherwise} \end{cases} \qquad \ldots\ldots 4.2$$

where $0 \le \gamma < 1$ is a reconstruction parameter arbitrarily chosen by the decoder.

The last step in reconstruction of the image is the inverse two-dimensional DOST. Note that the forward and inverse DOST have been discussed in Chapter three. The block diagram of the reconstruction/decompression process is shown in Figure 4.2.

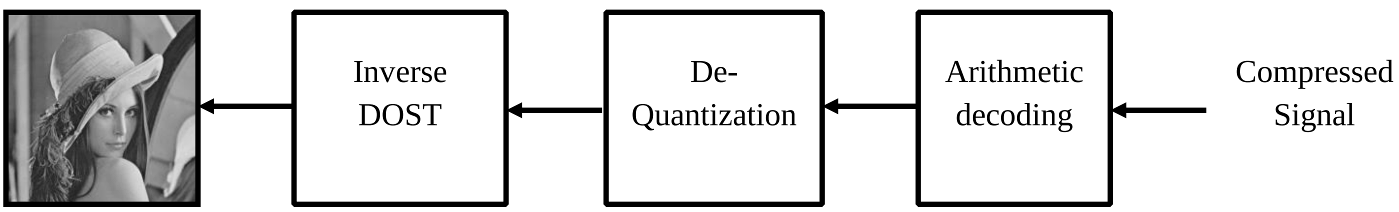

Figure 4.2 The decompression process by the proposed algorithm.

4.2 Performance Measurement Parameters

After reconstruction/decompression of the image, the quality of the image and the performance of the compression algorithm has to be tested. Therefore, the amount of compression and how good the reconstructed image is similar to the original is known from the test conducted. In this thesis the test was conducted by calculating important distortion measures namely: the mean square error (MSE), peak signal-to-noise ratio (PSNR) measured in decibels (dB), the compression ratio (CR) and structural similarity index (SSIM) which are all briefly defined below.

4.2.1 Mean Square Error (MSE)

The MSE is the cumulative squared error between the compressed and the original image. It measures the average of the square of the error. A lower value of MSE means lesser error.

$$MSE = \frac{1}{mn}\sum_{y=1}^{m}\sum_{x=1}^{n}\left[h(x,y) - h'(x,y)\right]^2 \quad \ldots\ldots 4.3$$

4.2.2 Peak Signal to Noise Ratio (PSNR)

PSNR is a measure of the peak error. Many signals have very wide dynamic range, because of that reason PSNR is usually expressed in terms of the logarithmic decibel scale (dB). A higher value of PSNR means higher signal to noise ratio. Values for PSNR range between infinity for identical images, to 0 for images that have no commonality. The PSNR is given as:

$$PSNR = 10\log_{10}\left\{\frac{\max h(x,y)^2}{MSE}\right\} = 20\log_{10}\left\{\frac{\max h(x,y)}{\sqrt{MSE}}\right\} \quad \ldots\ldots 4.4$$

where, $\max h(x,y)$ is the maximum possible pixel value of the image.

4.2.3 Compression Ratio (CR)

It is the measure of the reduction of the detailed coefficient of the data. In the process of image compression, it is important to know how much detailed (important) coefficient one can discard from the input data in order to sanctuary critical information of the original data. Compression ratio can be expressed as:

$$CR = \frac{size\,of\ compresed\,image}{size\,of\ original\,image} \quad \ldots\ldots 4.5$$

4.2.4 Structural Similarity Index (SSIM)

SSIM is the structure similarity index for measuring the similarity between the original image and compressed image. Given two image signals or pixels x and y from two images, which are aligned with each other, the SSIM between the two image signals is given as a function of three characteristics which are luminance *l(x,y)*, contrast *c(x,y)* and structure *s(x,y)*. SSIM lies between 0 and 1.

$$SSIM(x,y) = f(l(x,y), c(x,y), s(x,y))$$

$$l(x,y) = \frac{2\mu_x\mu_y + C_1}{\mu_x^2 + \mu_y^2 + C_1} \qquad \text{4.6}$$

where μ_x and μ_y are the mean intensities and C_1 is a non-negative constant,

$$c(x,y) = \frac{2\sigma_x\sigma_y + C_2}{\sigma_x^2 + \sigma_y^2 + C_2} \qquad \text{4.7}$$

where σ_x and σ_y are the standard deviations and C_2 is a non-negative constant,

$$s(x,y) = \frac{\sigma_{xy} + C_3}{\sigma_x\sigma_y + C_3} \qquad \text{4.8}$$

where $\sigma_{xy} = \frac{1}{N-1}\sum_{i=0}^{N}(x_i - \mu_x)(y_i - \mu_y)$, where *N* is the number of signal samples (pixels) and C_3 is a non-negative constant.

Using equations (4.6), (4.7) and (4.8) the SSIM is given as:

$$SSIM(x,y) = \frac{(2\mu_x\mu_y + C_1)(2\sigma_{xy} + C_2)}{(\mu_x^2 + \mu_y^2 + C_1)(\sigma_x^2 + \sigma_y^2 + C_2)} \qquad \text{4.9}$$

Chapter Five

Results and Discussion

The proposed compression scheme was implemented on an intel® core (TM) i5-6200U processor, CPU: 2.30 GHZ and 4 GB RAM computer. All tests were carried out on a Matlab R2015b platform. The medical images used for testing the algorithm were all taken from a publicly available database found at http://sun.aei.polsl.pl/~rstaros/mednat/index.html. The images available on the database were used to evaluate the performance of lossless image compression algorithms for medical and natural continuous tone grayscale images. The image compression was applied on 12 computed radiography images, 12 ultrasound images, 12 MRI images and 12 CT scan images as well as common test images including the well-known 512 x 512, 8 bit per pixel grayscale test image of Lena. The compressed images are compared against the originals to measure image quality. PSNR, MSE, CR and SSIM have been used as performance measurement parameters. The proposed DOST transform based image compression scheme has been compared with that of DCT and Haar wavelet transform based image compression techniques. The efficacy of each compression scheme is measured in terms of the performance measuring parameters. The different transform-based compression schemes, the performance measurement parameters, quantization and entropy coding are all discussed in the previous chapters.

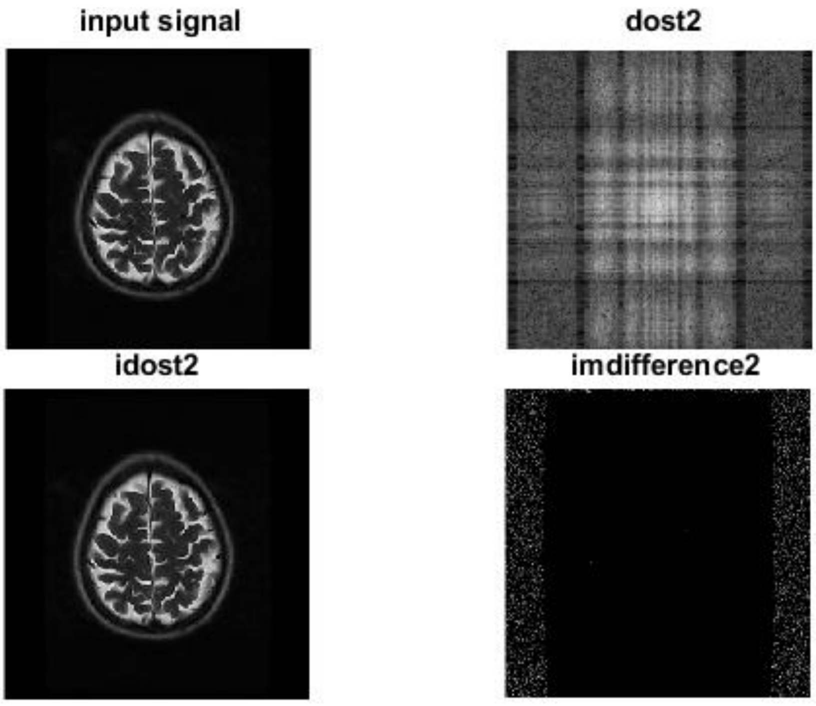

Figure 5.1 Proposed DOST based image compression scheme applied on an MRI brain image: original image (top left), its discrete DOST amplitude spectrum (top right), recovered image after decompression (bottom left) and the difference between the original and decompressed image (bottom right).

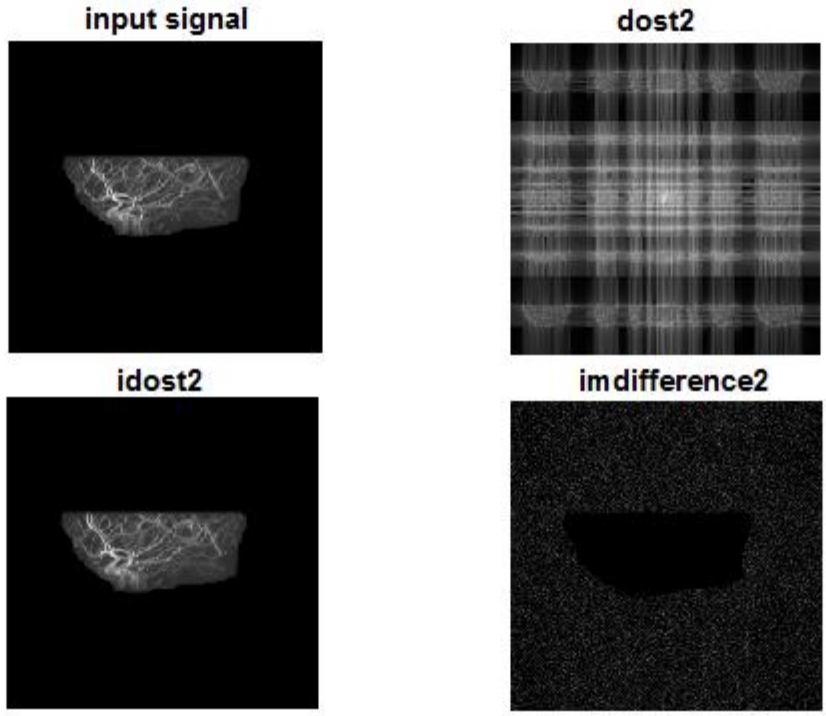

Figure 5.2 Proposed DOST based image compression scheme applied on an angiogram image: original image (top left), its discrete DOST amplitude spectrum (top right), recovered image after decompression (bottom left) and the difference between the original and decompressed image (bottom right).

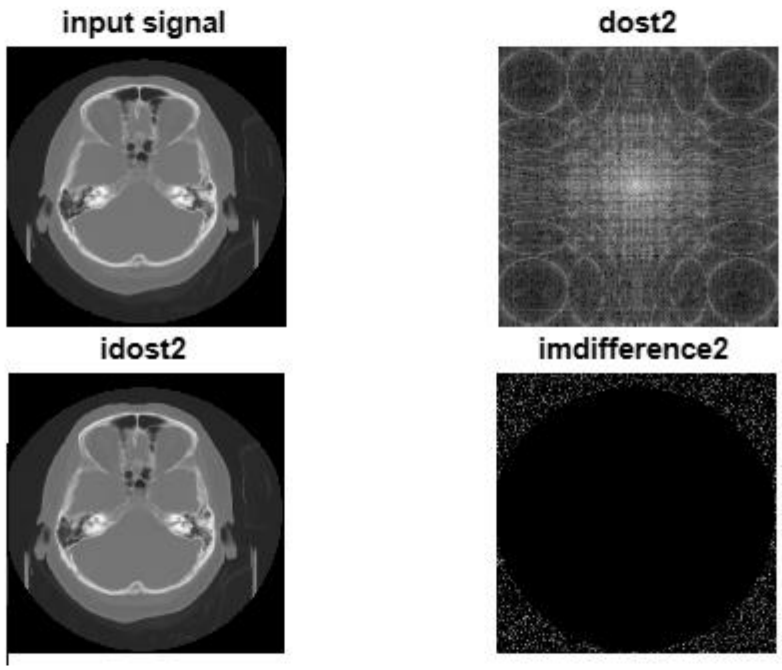

Figure 5. 3 Proposed DOST based image compression scheme applied on a CT scan image: original image (top left), its discrete DOST amplitude spectrum (top right), recovered image after decompression (bottom left) and the difference between the original and decompressed image (bottom right).

Figures 5.1, 5.2 and 5.3 present pictorial results found after the proposed compression scheme has been applied on typical MRI, angiogram and CT images. The original images, their DOST amplitude spectrum, the decompressed images (after the application of the inverse DOST) as well as the difference between the original and decompressed images are all shown. The difference has been plotted to visually assess the amount of information loss during the compression-decompression process. Generally, the difference images are mostly filled with dark pixels and noise components which do not actually carry much imaging signal information. Significant loss of information during the compression-decompression process in our case is not acceptable as it might make image-based diagnosis very difficult (as we are dealing with medical images).

As mentioned earlier, 12 computed radiography image, 12 ultrasound images, 12 MRI images and 12 CT scan images have been used for testing the performance of the proposed algorithm. Using the proposed DOST based image compression scheme, 9 MRI images were found with a SSIM values more than 0.9997. The rest were found more than 0.7773. The minimum PSNR achieved was 38.7370 which was for brain angiography. This image resulted in maximum MSE which was 35.0622. The second lowest PSNR value found was 44.74 and its MSE was 8.7989. The rest of the images achieved PSNR values greater than 50.00 and MSE less than 2.2553.

Using the DCT based image compression scheme, 9 MRI images were found with a SSIM more than 0.9899 and the rest were more than 0.7773. The minimum MSE achieved using the DCT based image compression scheme was 8.2983 and the maximum was 8.3460. The rest of the images had MSE values between 8.2983 and 8.3460. The PSNR in the DCT based image compression was almost similar with 44.9954 maximum and 44.9706 minimum values.

For the Wavelet based image compression scheme, Haar wavelet with two decomposition level was used. The reason for choosing the Haar wavelet was the fact that it is the simplest. In this case, 8 MRI images received a SSIM more than 0.9987 and the rest three images were between 0.8997 and 0.9987. The minimum PSNR found was 35.7370 with MSE of 36.1622 and the maximum was 48.5589 with MSE of 7.4377.

Tables 5.1, 5.2 and 5.3 present performance measurements of the proposed DOST based image compression scheme against DCT as well as wavelet-based methods for selected MRI images. It is clear that the proposed method in this thesis generally outperforms both the DCT as well as wavelet-based methods in most cases.

Name of the Image	Original Medical Image	Decompressed Medical Image	PSNR	MSE	CR	SSIM
mr_2321	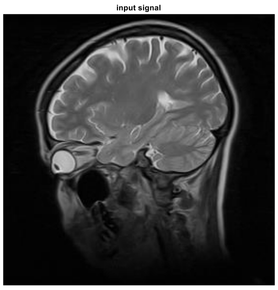	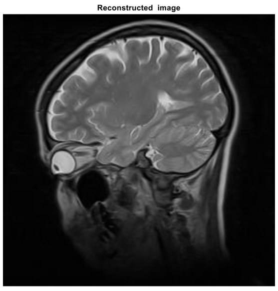	44.7411	8.7989	69.6392	0.9998
mr_6624	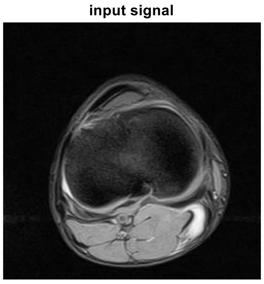		50.46	2.36	45.6541	1
mr_2412		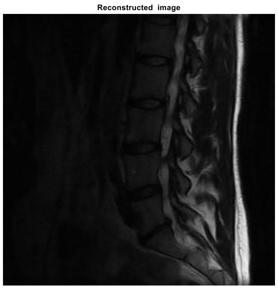	50.6533	2.2553	71.7096	0.9999
mr_2896	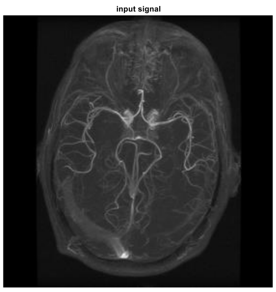	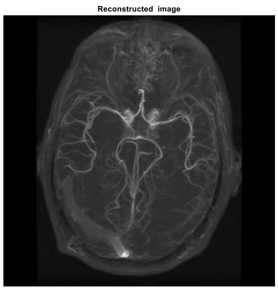	38.737	35.062	62.6392	0.7773
mr_2337	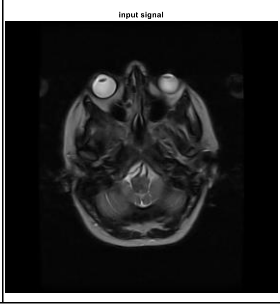	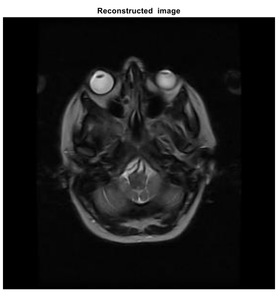	50.5959	2.2853	43.5947	0.7821

Table 5.1 Performance measurement for the proposed DOST based image compression of MRI images.

Name of the Image	Original Medical Image	Decompressed Medical Image	PSNR	MSE	CR	SSIM
mr_2321	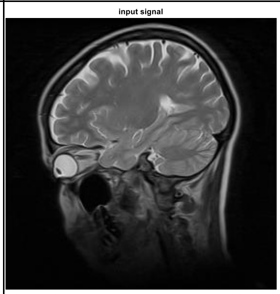		44.9754	8.3367	59.7489	0.9997
mr_6624	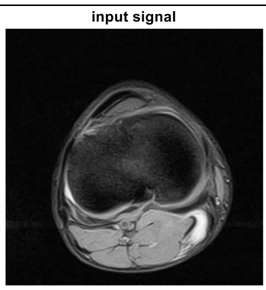	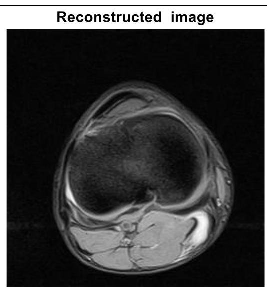	44.9954	8.2984	43.5419	0.9999
mr_2414			44.9711	8.345	68.0196	0.9999
mr_2896	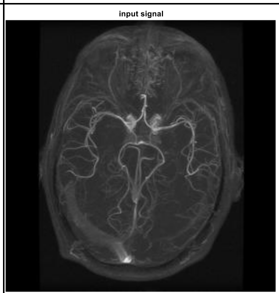	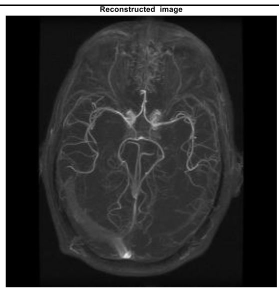	44.9706	8.3459	33.7539	0.7789
mr_2337	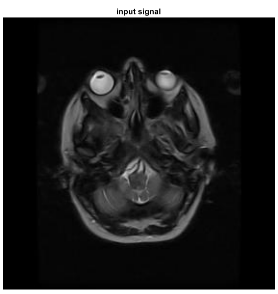	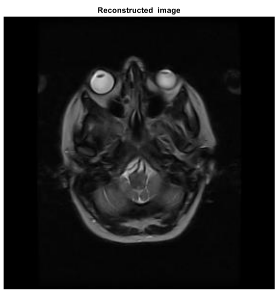	44.9619	8.3627	53.5419	0.7809

Table 5.2 Performance measurement for DCT based image compression of MRI images.

Name of the Image	Original Medical Image	Decompressed Medical Image	PSNR	MSE	CR	SSIM
mr_2321	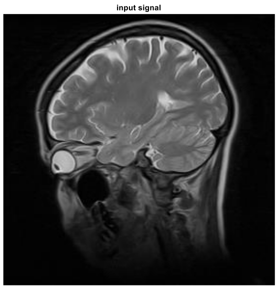	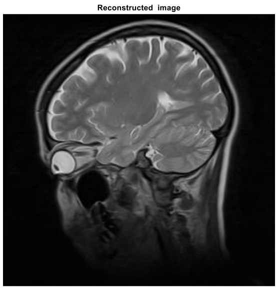	46.7954	8.1857	63.3592	0.9987
mr_6624	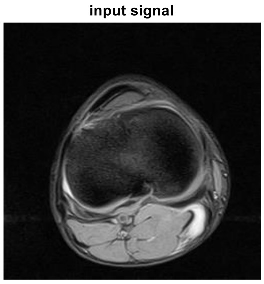		45.9831	8.2954	42.4418	0.9899
mr_2414		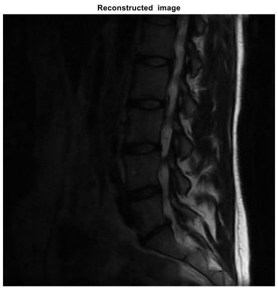	44.3029	8.7723	73.1175	0.9769
mr_2896	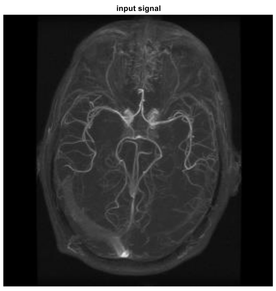	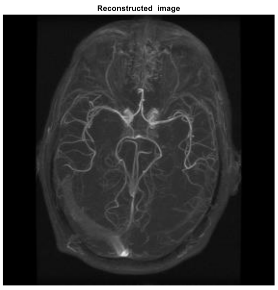	35.737	36.1622	41.589	0.7796
mr_2337	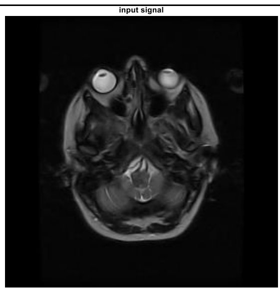	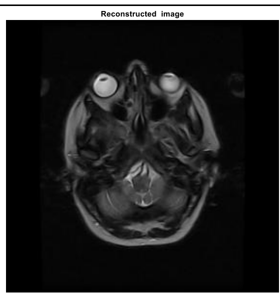	48.5589	7.4377	62.6589	0.8809

Table 5.3 Performance measurement for wavelet based image compression of MRI images.

Out of the 12 CT scan images considered, the DOST image compression scheme received SSIM more than 0.8166 for 8 images, 1.000 for 3 images and 0.5564 for 1 of the images. The minimum PSNR was 44.7747 and the maximum was 50.6509. The smallest MSE was 2.2566 and the largest was 9.1959. While 9 of the images received MSE between 4.8281 and 2.2566.

Out of the total, 9 of the CT images received SSIM more than 0.8166 and the rest were between 0.7773 and 0.8166 using the DCT based image compression scheme. The minimum MSE was found to be 8.2983 and the maximum was 8.3340. The PSNR was almost uniform ranging from 44.9768 to 44.9853.

The wavelet-based image compression scheme applied on the CT images received SSIM of all greater than 0.8166. The minimum PSNR was 44.8817with MSE of 8.2246 and the maximum was 49.7056 with MSE of 6.2143.

Tables 5.4, 5.5 and 5.6 present comparisons between proposed method, DCT based and that of wavelet-based compression schemes applied on selected CT images. As shown in the table, the compression ratios computed for DOST were higher than both wavelet and DCT based schemes (same for the MRI images considered above).

Name of the Image	**Original Medical Image**	**Decompressed Medical Image**	**PSNR**	**MSE**	**CR**	**SSIM**
ct_4006	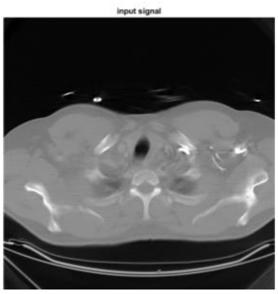	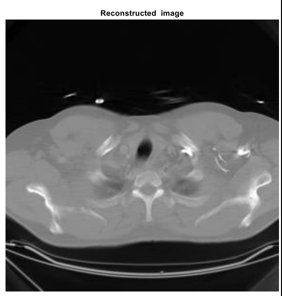	50.6509	2.2566	53.1584	1
ct_29920		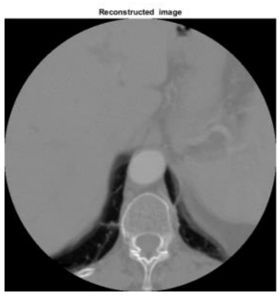	47.3392	4.8375	45.2658	0.8170

ct_17			47.3476	4.8281	61.2148	0.8169
ct _4087	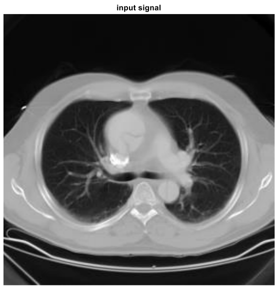	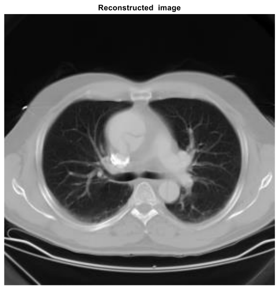	44.7747	8.7311	64. 5462	1
ct_4165		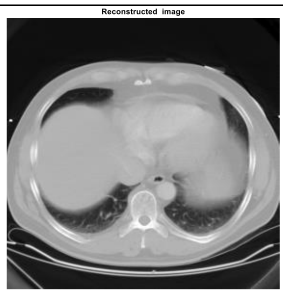	44.7993	8.6817	53.1548	1

Table 5.4 Performance measurement for DOST based image compression of CT scan images.

Name of the Image	Original Medical Image	Decompressed Medical Image	PSNR	MSE	CR	SSIM
ct_4006	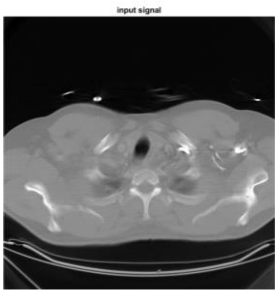	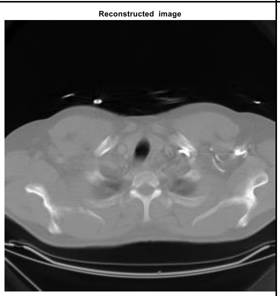	44.9821	8.3240	33.6774	0.9999
ct_29920	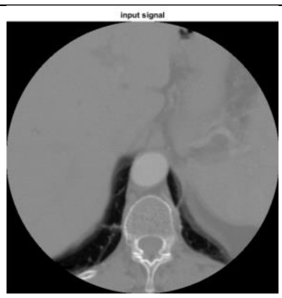	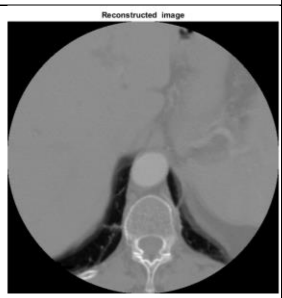	44.9768	8.3340	53.5419	0.8168

ct_17	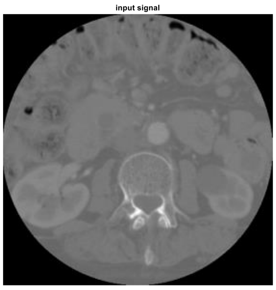		44.9853	8.3178	53.8569	0.8166
ct _4087	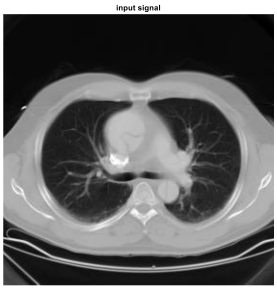	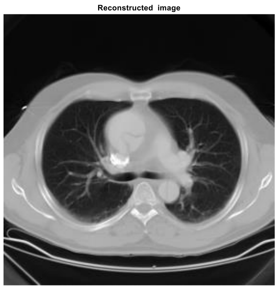	44.977	8.3337	62.2533	0.9999
ct_4165		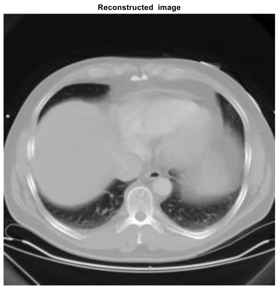	44.9817	8.3246	33.2459	0.9999

Table 5.5 Performance measurement for DCT based image compression of CT scan images.

Name of the Image	**Original Medical Image**	**Decompressed Medical Image**	**PSNR**	**MSE**	**CR**	**SSIM**
ct_4006	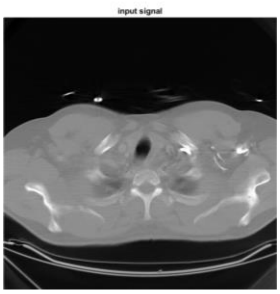	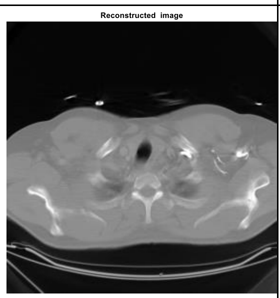	49.7056	6.2143	67.5684	0.9996
ct_29920			46.5267	8.2352	69.2578	0.8667

ct_17	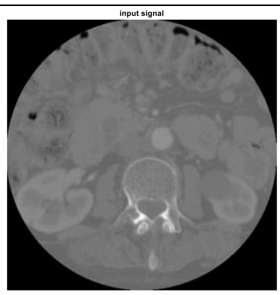		44.9853	8.3178	60.5924	0.8166
ct _4087	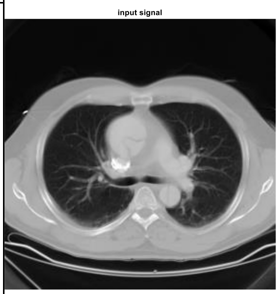	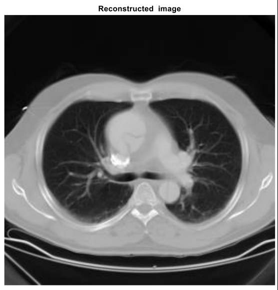	45.9769	8. 3961	49.3871	0.9997
ct_4165	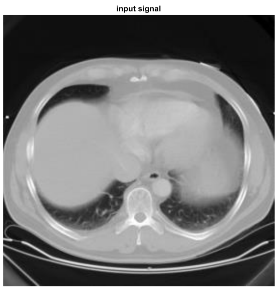		44.8817	8.2246	58.5473	0.9999

Table 5.6 Performance measurement for wavelet based image compression of CT scan images.

Compared to the MRI and CT images considered, the compression-decompression procedure applied on the ultrasound and computed radiography images offered less impressive results. Typical of the CR and US images is that both are noisy and often of low dynamic range. Figures 5.4 and 5.5 present two such cases. The recovered images appeared quite fuzzy compared to the original input images. The proposed DOST based algorithm might need some modifications to address the issues observed. The image difference between the input and recovered signals do not seem to contain that much useful information. But the fact that the recovered image is of less quality than the original by itself is alarming. As we are dealing with medical images, we cannot afford to lose too much information as image based diagnostic procedures rely on the quality of the images being assessed. Off course no one could claim to develop a compression scheme that works best for any medical image.

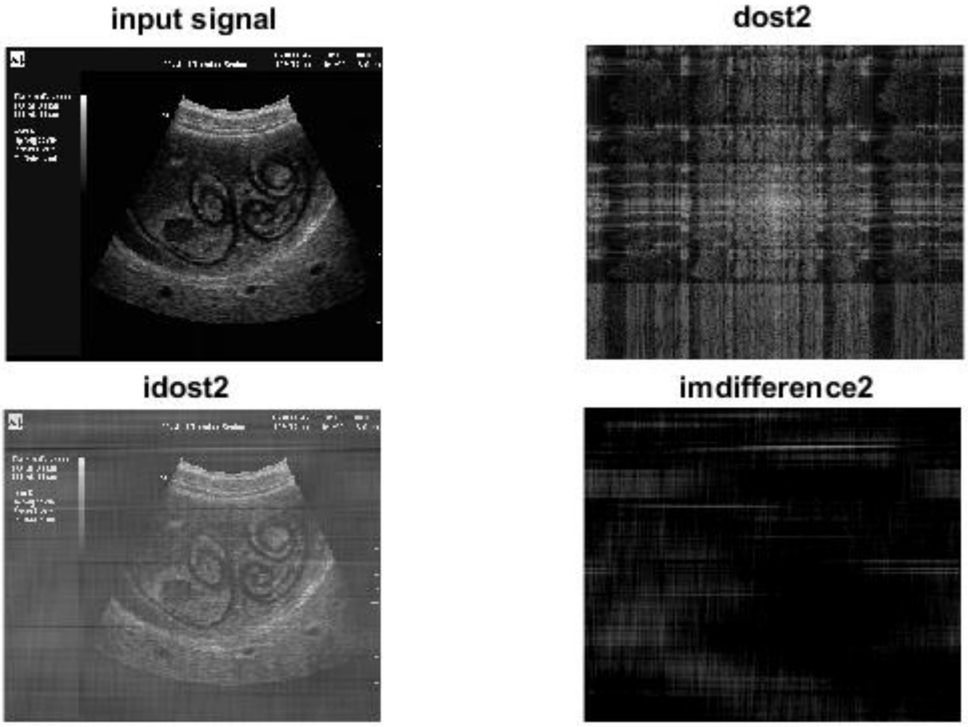

Figure 5.4 Proposed DOST based image compression scheme applied on an ultrasound image: original image (top left), its discrete DOST amplitude spectrum (top right), recovered image after decompression (bottom left) and the difference between the original and decompressed image (bottom right).

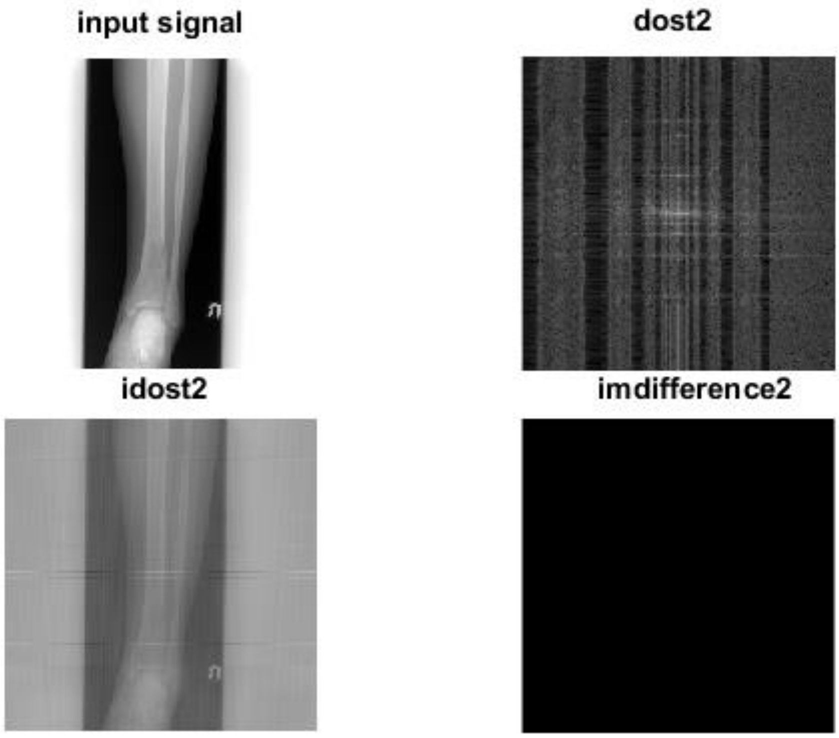

Figure 5.5 Proposed DOST based image compression scheme applied on a computed radiography image: original image (top left), its discrete DOST amplitude spectrum (top right), recovered image after decompression (bottom left) and the difference between the original and decompressed image (bottom right).

Table 5.7 and 5.8 show the decompression results of CT scan images using the three compression schemes.

Name of the Image	Original Medical Image	Decompressed Medical Image Using DOST	Decompressed Medical Image Using WT	Decompressed Medical Image Using DCT
ct_4006	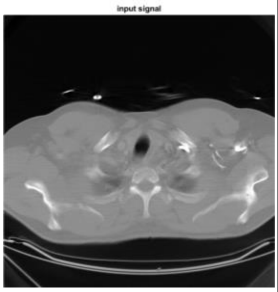	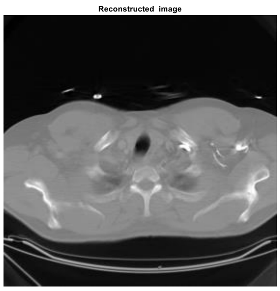	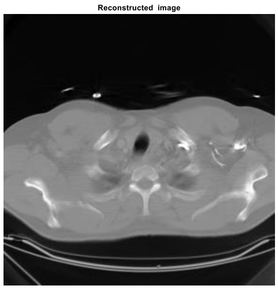	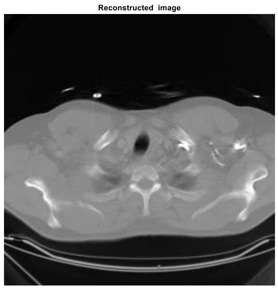
ct_29920				
ct_17		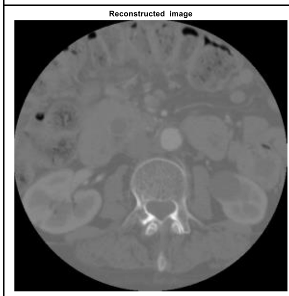		
ct _4087				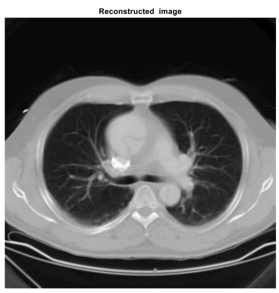
ct_4165				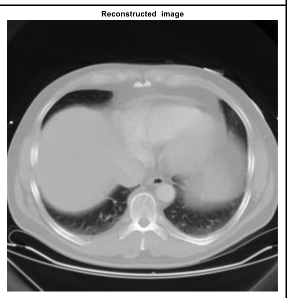

Table 5.7 Decompressed CT-scan image using the three-image compression technique

Name of the Image	PSNR Using DOST	MSE Using DOST	CR Using DOST	SSIM Using DOST	PSNR Using WT	MSE Using WT	CR Using WT	SSIM Using WT	PSNR Using DCT	MSE Using DCT	CR Using DCT	SSIM Using DCT
ct_4165	44.7993	8.6817	53.1548	1.0000	44.8817	8.2246	58.5473	0.9999	44.9817	8.3246	33.2459	0.9999
ct 4087	44.7747	8.7311	64.5462	1.0000	45.9769	8.3961	49.3871	0.9997	44.9770	8.3337	62.2533	0.9999
ct_17	47.3476	4.8281	61.2148	0.8169	44.9853	8.3178	60.5924	0.8166	44.9853	8.3178	53.8569	0.8166
ct29920	47.3392	4.8375	45.2658	0.8170	46.5267	8.2352	69.2578	0.8667	44.9768	8.334	53.5419	0.8168
ct_4006	50.6509	2.2566	53.1584	1.0000	49.7056	6.2143	67.5684	0.9996	44.9821	8.324	33.6774	0.9999

Table 5.8 Performance measurement of CT-scan image using the three-image compression technique

Chapter Six

Conclusion and Future Works

This thesis presented an S transform-based scheme for use in efficient and effective compression of medical images. The performance of the proposed compression scheme is quantified in terms of useful matrices including compression ratio, mean square error, peak signal to noise ratio and structural similarity index. The proposed scheme has been tested on medical images generated from four image modality types: MRI, CT, ultrasound and computed radiograph. The overall performance of the proposed scheme appeared quite promising. Even though we used a lossy compression technique, which lead to loss of some information, the loss is considered diagnostically insignificant as confirmed by a radiologist. The amount of loss is examined by the radiologist. The lossy approach greatly reduces the cost of data storage and transmission to use the proposed scheme in telemetry applications.

The proposed scheme has been compared with other integral transform-based schemes including discrete Cosine transform and wavelets and found to be mostly superior to both. The proposed scheme achieved an average PSNR value of 47.0099 which is better compared to both DCT (which has an average PSNR of 41.9787) and Haar wavelet-based image compression technique (which offered an average PSNR of 42.9151). The average MSE achieved using the proposed algorithm was 8.0097 which is much better to that of Haar wavelet (8.2633) and DCT (8.3328) based methods. The average compression ratio with the proposed algorithm was 50.6031 and the structure similarity index was 0.9295. DCT had an average of 43.2928 compression ratio and 0.9192 structure similarity index while the wavelet-based image compression scheme offered an average of 49.8519 compression ratio and 0.9108 structure similarity index. The higher the PSNR the higher the image quality. The structural similarity index lies between 0 and 1. The value nearest to 1 means the reconstructed image is identical to the original image. The larger the MSE value the smaller the PSNR resulting in poor image quality.

As both the wavelet and S-transform based approaches make use of the multi-resolution concept, both are preferred over the DCT based approach. The S transform comes with even more interesting properties: it keeps the absolutely-referenced phase information and is less noisy compared to wavelets. Furthermore, due to the direct relationship of the S transform with the natural Fourier transform, its implementation is rather straightforward compared to wavelets.

Even though the proposed S transform-based approach offered promising results for use in effective and efficient medical image compression, there are still rooms for improvement. As seen on the results section, its performance when applied on ultrasound and computed radiography images requires improvement. Also, there are new models of entropy coding and quantization proposed in the literature and utilizing those could improve further the performance of the proposed scheme. Furthermore, the use of S transform in developing lossless compression schemes need further investigation. Also, the scheme ought to be tested on medical images acquired from other imaging modality types than those considered in this thesis. The clinical implications of the method should also have to be checked rigorously. This and similar other issues await further studies.

Reference

1. The Royal Australian and New Zealand College of Radiologist, “A Guideline for the Use of Image Compression in Diagnostic Imaging”, Nov 5, 2010.
2. R. Norcen, M. Podesser, A. Pommera, H.-P. Schmidt, A. Uhla, “Confidential Storage and Transmission of Medical Image Data”, Computers in Biology and Medicine, pp. 277–292, 2003.
3. M. Ferni Ukrit, A. Umamageswari, G. R. Suresh, “A Survey on Lossless Compression for Medical Image”’, International Journal of Computer Application (0975-8887), Volume 31-No 8, October 2011.
4. K. Admasu, A. Tamire, and S. Tsegaye, “Envisioning the Future of the Health Sector: an Update”, Federal Ministry of Health, Ethiopia, 2015
5. A. Alarabeyyat, S. Al-Hashemi, T. Khdour, M. Hjouj Btoush, S. Bani-Ahmad, R. Al-Hashemi., “Lossless Image Compression Technique Using Combination Methods”, Journal of Software Engineering and Application, October 2012.
6. D. A. Karras, S. A. Karkanis, and D. E. Maroulis, “Efficient Image Compression of Medical Images Using the Wavelet Transform and Fuzzy C-Means Clustering on Regions of Interest”, IEEE 1089-6503, 2000.
7. S. Cho, D. Kim, and W. A. Pearlman, “Lossless Compression of Volumetric Medical Images with Improved 3-D SPIHT Algorithm”, Journal of Digital Imaging, January 2004.
8. S. M. Ramesh, A. Shanmugam, “Medical Image Compression Using Wavelet Decomposition for Prediction Method”, International Journal of Computer Science and Information Security, Vol 7, No 1, 2010.
9. B. C. Vemuri, S. Sahni, C. Kapoor, and J. Fitzsimmons, “Lossless Image Compression”, University of Florida, 2007.
10. L. Yun, X. Xiaochun, L. Bin and P. Jinfeng, “Time-Frequency Analysis Based on the S-Transform”, International Journal of Signal Processing, Image Processing and Pattern Recognition, Volume 6, No 5, 2013.
11. Y. H. Wan, The Tutorial: S Transform, Graduate Institute of Communication Engineering National Taiwan University, 2010.
12. M. Vaishnav, C. Kamargaonkar and M. Sharma, “Medical Image Compression Using Dual Tree Complex Wavelet Transform and Arithmetic Coding Technique”, International Journal of Scientific Research in Computer Science, Engineering and Information Technology, Volume 2, Issue 3, 2017.
13. T. H. Henry Lee, Introduction to Medical Image Compression Using Wavelet Transform, National Taiwan University, Dec. 31, 2007.
14. M. J. Zukoski, T. Boult and T. Iyriboz, “A Novel Approach to Medical Image Compression”, International Journal of Bioinformatics Research and Applications, Vol. 2, No. 1, 2006.

15. G. Gupta, P. Thakur, "Image Compression Using Lossless Compression Techniques", International Journal on Recent and Innovation Trends in Computing and Communication, ISSN 2321-8169, Volume 2, Issue 12, December 2014.
16. V. Panigrahy, "Lossless Image Compression and Secure Storage of Medical Images", NIT Rourkela Department of Computer Science and Engineering National Institute of Technology Rourkela, Orissa, May 2012.
17. Sindhu M. S, Bharathi S. H., "Image Compression Using Haar Wavelet Transform and Huffman Coding", International Journal of Research and Scientific Innovation, ISSN 2321 – 2705, Volume 3, Issue 5, May 2016.
18. N. Kaur, "A Review of Image Compression Using Pixel Correlation and Image Decomposition with Results", International Journal of Application or Innovation in Engineering & Management, ISSN 2319-4847, Volume 2, Issue 1, January 2013.
19. S. Sachdeva, R. Kaur, "A Review on Digital Image Compression Techniques", International Journal on Recent and Innovation Trends in Computing and Communication, Volume 2, Issue 7, July 2014
20. R. C. Gonzalez and R. E. Woods, Digital Image Processing (Second Edition), Prentice Hall, pp. 409-518.
21. A. Deshlahra, "Analysis of Image Compression Methods Based on Transform and Fractal Coding", National Institute of Technology, Rourkela. May 2013.
22. S. A. Khayam, "The Discrete Cosine Transform (DCT): Theory and Application", Department of Electrical & Computer Engineering, Michigan State University, March 10th 2003.
23. Y. Wang, "Efficient Stockwell Transform with Applications to Image Processing", University of Waterloo, Waterloo, Ontario, Canada, 2011.
24. D. Assefa, "The 1D and 2D Localized Hartley Transforms Their Parallel Implementation and Applications; Color Image Analysis Using Quaternions and Trinions", The University of Western Ontario London, Ontario, pp. 15-19, August 2007.
25. Nithya B, Y. B. Sankari, Manikantan K, S. Ramachandran, "Discrete Orthonormal Stockwell Transform Based Feature Extraction for Pose Invariant Face Recognition", International Conference On Advanced Computing Technologies and Applications, pp. 290-299, 2015.
26. J. Ladan, "An Analysis of Stockwell Transforms, With Applications to Image Processing", University of Waterloo, Ontario, Canada, 2014.
27. S. Saoud, S. Bousselmi, M. B. Naser, A. Cherif, "New Speech Enhancement Based On Discrete Orthonormal Stockwell Transform", International Journal of Advanced Computer Science and Applications, Vol. 7, No. 10, 2015.
28. Y. Wang and J. Orchard, "The Discrete Orthonormal Stockwell Transform for Image Restoration", International Conference IEEE, 2009.

29. M. A. T. Figueiredo, Scalar and Vector Quantization, Department of Electro-technical and Computer Engineering, Technichal Intitute of Superior, Portugal, November 2008.
30. M. W. Marcellin, M. A. Lepley, Ali Bilgin, Thomas J. Flohr, Troy T. Chinen, James H. Kasner, "An Overview of Quantization in JPEG2000", Signal Processing: Image Communication, pp. 73–84, 2002.
31. M. Rabbani, R. Joshi, "An Overview of The JPEG2000 Still Image Compression Standard", Signal Processing: Image Communication, pp. 3–48, Volume 17, Issue 1, 2002.
32. C. Lui, "A Study of the JPEG-2000 Image Compression Standard", Queen's University, Kingston, May 2001.
33. R. R. Coifman, Y. Meyer, M. V. Wickerhauser, "Wavelet Analysis and Signal Processing in Wavelets and Their Applications", Jones and Bartlett, Boston, pp. 153-178, ISBN 0-86720-225-4, 1992.
34. X. Mi, H. Ren, Z. Ouyang, W. Wei1 and K. Ma, "The Use of the Mexican Hat and the Morlet Wavelets for Detection of Ecological Patterns", Plant Ecol, ISSN 1385-0237, 2005.
35. A. Bernardino, J. Santos-Victor, "A Real-Time Gabor Primal Sketch for Visual Attention", Iberian Conference on Pattern Recognition and Image Analysis, pp. 335-342, volume 3522, 2005.
36. T. Acharya, P. S. Tsai, JPEG2000 Standard for Image Compression Concepts, Algorithms and VLSI Architectures, John Wiley & Sons, 2005.
37. D. V. Rojatkar, N. D.Borkar, B. R. Naik, R. N. Peddiwar, "Image Compression Techniques: Lossy and Lossless", International Journal of Engineering Research and General Science, ISSN 2091-2730, Volume 03, Issue 02, April, 2015.
38. B. Gupta, "Study of Various Lossless Image Compression Technique", International Journal of Emerging Trends & Technology in Computer Science, ISSN 2278-6856, Volume 02, Issue 04, August 2013.
39. G. Gupta, P. Thakur, "Image Compression Using Lossless Compression Techniques", International Journal on Recent and Innovation Trends in Computing and Communication ISSN: 2321-8169, Volume 2, Issue 12, 3896 – 3900, December 2014.
40. P. V. Shantagiri1 and Saravanan, "Pixel Size Reduction Lossless Image Compression Algorithm", International Journal of Computer Science & Information Technology, Vol 5, No 2, April, 2013.
41. G. Vijayvargiya, S. Silakari, R. Pandey, "A Survey: Various Techniques of Image Compression", International Journal of Computer Science and Information Security, Volume 11, No. 10, October 2013.
42. W. Z. Wahba, A. Y. A. Maghari, "Lossless Image Compression Techniques Comparative Study", International Research Journal of Engineering and Technology (IRJET), e-ISSN: 2395-0056, Volume 03, Issue 02, Feb 2016.